Atmos. Chem. Phys. Discuss., 12, 15743–15799, 2012
www.atmos-chem-phys-discuss.net/12/15743/2012/
doi:10.5194/acpd-12-15743-2012

Atmospheric Chemistry and Physics Discussions

The influence of snow grain size and impurities on the vertical profiles of actinic flux and associated NO_x emissions on the Antarctic and Greenland ice sheets

M. C. Zatko[1], T. C. Grenfell[1], B. Alexander[1], S. J. Doherty[2], J. L. Thomas[3,4], and X. Yang[5,6]

[1]Department of Atmospheric Sciences, Box 351640, University of Washington, Seattle, WA 98195, USA
[2]Joint Institute for the Study of Atmosphere and Ocean, 3737 Brooklyn Ave NE, Seattle, WA 98195, USA
[3]UPMC Univ. Paris 06, UMR8190, CNRS/INSU – Université Versailles St.-Quentin, LATMOS-IPSL, Paris, France
[4]University of California, Los Angeles; Department of Atmospheric and Oceanic Sciences, Los Angeles, CA 90095, USA
[5]National Centre for Atmospheric Science (NCAS), Cambridge, CB2 1EW, UK
[6]Centre for Atmospheric Science, Department of Chemistry, University of Cambridge, Cambridge CB2 1EW, UK

Received: 17 March 2012 – Accepted: 31 May 2012 – Published: 26 June 2012

Correspondence to: B. Alexander (beckya@atmos.washington.edu)

Published by Copernicus Publications on behalf of the European Geosciences Union.

ACPD
12, 15743–15799, 2012

Abstract

We use observations of the absorption properties of black carbon and non-black-carbon impurities in near-surface snow collected near the research stations at South Pole and Dome C, Antarctica and Summit, Greenland combined with a snowpack actinic flux parameterization to estimate the vertical profile and e-folding depth of ultraviolet/near-visible (UV/near-vis) actinic flux in the snowpack at each location. We have developed a simple and broadly applicable parameterization to calculate depth and wavelength dependent snowpack actinic flux that can be easily integrated into large scale (e.g. 3-D) models of the atmosphere. The calculated e-folding depths of actinic flux at 305 nm, the peak wavelength of nitrate photolysis in the snowpack, are 8–12 cm near the stations and 15–31 cm away (>11 km) from the stations. We find that the e-folding depth is strongly dependent on impurity content and wavelength in the UV/near-vis region, which explains the relatively shallow e-folding depths near stations where local activities lead to higher impurity levels. We calculate the lifetime of NO_x in the snowpack interstitial air produced by photolysis of snowpack nitrate against escape (τ_{escape}) from the snowpack via diffusion and windpumping and compare this to the calculated lifetime of NO_x against chemical conversion to HNO_3 ($\tau_{chemical}$) to determine whether the NO_x produced at a given depth can escape from the snowpack to the overlying atmosphere. Comparison of τ_{escape} and $\tau_{chemical}$ suggests efficient escape of photoproduced NO_x in the snowpack to the overlying atmosphere. Calculated vertical actinic flux profiles and observed snowpack nitrate concentrations are used to determine the flux of NO_x from the snowpack. Calculated NO_x fluxes of 4.4×10^8–2.8×10^9 molecules $cm^{-2}\,s^{-1}$ in remote polar locations and 3.2–8.2×10^8 molecules $cm^{-2}\,s^{-1}$ near polar stations for January at Dome C and South Pole and June at Summit suggest that NO_x flux measurements near stations are likely underestimating the amount of NO_x emitted from the clean, polar snowpack by a factor of 1.4–2.4.

ACPD
12, 15743–15799, 2012

1 Introduction

Research over the past two decades has provided ample evidence that unique photochemical reactions occur in snow-covered regions during periods of sunlight (Domine and Shepson, 2002; Grannas et al., 2007 and references within; Honrath et al., 1999). The photolysis of chemical species present in the snowpack, such as nitrate (NO_3^-), hydrogen peroxide (H_2O_2), formaldehyde (CH_2O), and nitrous acid (HONO), is a source of oxidants (NO_2, OH, O_3, HO_2) to the atmosphere within and above the snowpack (Beine et al., 2002; Beyersdorf et al., 2007; Cotter et al., 2003; Davis et al., 2001, 2004; Dibb et al., 2002; France et al., 2011; Frey et al., 2009; Honrath et al., 1999, 2002; Jones et al., 2001, 2007; Mauldin et al., 2010; Oncley et al., 2004; Sjostedt et al., 2007). Photochemical reactions in the snowpack have significant implications for the oxidizing capacity of the boundary layer over snow-covered regions (Chen et al., 2007; Grannas et al., 2007 and references within; Sjostedt et al., 2007; Thomas et al., 2012) and for the preservation of trace species such as NO_3^-, H_2O_2, and organics in ice cores (Mulvaney et al., 1998).

The formation and deposition of atmospheric nitrate (particulate NO_3^- and $HNO_3(g)$) is typically thought to be a permanent sink for gaseous NO_x ($NO_x = NO$ and NO_2) in the troposphere because gas-phase nitric acid $HNO_3(g)$ is not readily photolyzed at wavelengths (λ) > 325 nm (Johnston and Graham, 1973). However, nitrate deposited to the snowpack can be re-released to the atmosphere both by photolysis (as NO_x) (Davis et al., 2008; Honrath et al., 1999, 2002) and evaporation (as HNO_3) (Mulvaney et al., 1998) at depths below the snow surface followed by re-deposition to the surface snowpack (Rothlisberger et al., 2000). This is supported by observations of surface snow nitrate concentrations roughly an order of magnitude larger than nitrate concentrations at 10 cm depth in continental Antarctica snowpack (Dibb et al., 2004; Frey et al., 2009; Mayewski and Legrand, 1990; Rothlisberger et al., 2000) and by observations of an upward flux of NO_x out of the snowpack in polar regions on the order of $1.3–6.7 \times 10^8$ molecules cm^{-2} s^{-1} (Beine et al., 2002; Davis et al., 2004; Honrath et al.,

ACPD
12, 15743–15799, 2012

1999; Jones et al., 2001; Oncley et al., 2004). Following nitrate photolysis (photodenitrification), NO_x is transported from the snowpack interstitial air via diffusion and wind pumping, re-oxidized to HNO_3 in the atmosphere, and redeposited to the snowpack surface as NO_3^-. The results of earlier isotopic ($\delta^{15}N$) studies disagree on whether evaporation or photodenitrification is the dominant process of nitrate removal from the snowpack (Blunier et al., 2005; Savarino et al., 2007); but results from Frey et al. (2009) suggest that photodenitrification is the dominant contributor to post-depositional processing of NO_3^- in East Antarctica (Dome C). The dominance of photodenitrification is consistent with observations of downward fluxes of HNO_3 to the snowpack (Dibb et al., 2004). Although both NO_x and HONO are produced from NO_3^- photolysis, observations of the upward flux of NO_x above the snow surface at Summit, Greenland were roughly an order of magnitude larger than the measured flux of HONO (Dibb et al., 2004). Factors such as actinic flux, snow accumulation rate, snow acidity, and the gradient of temperature within the snow may influence the redistribution of snowpack nitrate (Rothlisberger et al., 2000). Here, actinic flux is defined as the irradiance impingent through a given point in all (4π) directions.

Several process-based modeling studies have calculated the flux of NO_x from the high-latitude snowpacks at Neumayer, Antarctica (Wolff et al., 2002), Ny-Ålesund, Svalbard (France et al., 2010), Summit, Greenland (Thomas et al., 2011), Dome C, Antarctica (France et al., 2011), and Barrow, Alaska (France et al., 2012). Estimates of depth-integrated snowpack actinic flux are required to model the flux of NO_x from the snowpack. Using surface irradiances from the British Antarctic Survey radiative transfer model (Gardiner and Martin, 1997) and a snowpack radiative transfer model (Grenfell, 1991), Wolff et al. (2002) calculated an e-folding depth of actinic flux in snowpack (z_e) of 3.7 cm at λ = 320 nm. This e-folding depth is now thought to be too shallow because those calculations used near-UV absorption coefficients of ice from Grenfell and Perovich (1981) and Perovich and Govoni (1991), which have since been superseded by much smaller values (Askebjer et al. 1997a,b; Warren et al., 2006). The earlier measurements overestimated the absorption coefficient of ice at blue and near-

ACPD
12, 15743–15799, 2012

UV wavelengths because they attributed attenuation of light in clear bubble-free ice as solely due to absorption, whereas in fact the attenuation had a significant contribution from Rayleigh scattering by lattice defects (Price and Bergström, 1997). The currently accepted UV absorption coefficients for ice are less than 0.1 m^{-1} (Warren et al., 2006). Measured and calculated z_e from later studies range from 6–9 cm at Ny-Ålesund, 10–20 cm at Dome C, and to 9–14 cm at Barrow (France et al., 2010, 2011, 2012).

We define z_e as the depth in the snowpack where the actinic flux is 1/e of the surface value. Snowpack z_e values are dependent upon snow physical and optical properties (e.g., grain size, bulk density, refractive index) as well as the type and concentration of impurities in the snow (e.g., black carbon). Pure ice is a moderate absorber of near-IR and a strong absorber of infrared radiation, but an extremely weak absorber of UV radiation, the latter of which is relevant for photochemistry. At UV and near-UV wavelengths, snow grains are much more efficient scatterers than absorbers; however, multiple scattering of radiation in the snowpack increases the probability of absorption by ice grains and impurities in the snow. Because ice is so weakly absorbing at these wavelengths, the absorption in natural snow is dominated by impurities, even in the cleanest snow. Dust, brown carbon, and Humic-Like-Substances (HULIS) also absorb radiation and have a much stronger wavelength dependence across the UV/near-vis compared to black carbon (BC) (France et al., 2011, 2012; Hoffer et al., 2006). However, while the optical properties of HULIS have been quantified in several studies (France et al., 2012; Hoffer et al., 2006; Kirchsetter et al., 2004; Roden et al., 2006) the range of optical properties for HULIS is large and the amount of HULIS in the Arctic and Antarctic snowpack has not been quantified.

Since snow impurities dominate absorption in the UV/near-vis λ range, here we use optical measurements of particulate material collected on filters through which snow meltwater had been passed. The snow samples were collected at Dome C and Summit; the filters were examined with a laboratory spectrophotometer (Grenfell et al., 2011), which was specifically designed to estimate the amount of BC verses nonBC absorption and amount of BC material in snowpacks. Samples were collected near Dome C

ACPD
12, 15743–15799, 2012

station and at remote sites more than 11 km from Dome C and Summit stations. We incorporate these impurity measurements into a simple parameterization to calculate depth-dependent actinic flux profiles in deep snowpack for λ between 289–850 nm in order to estimate the flux of NO_x from the snowpack via NO_3^- photolysis. The parameterization is derived (in Sect. 2.3 below) from a well-tested discrete ordinate method radiative transfer model for optically thick snow and ice (Grenfell, 1991), and can easily be incorporated into large-scale models such as global climate models and global chemical transport models. To estimate photolysis in the snow, we calculate the depth profile of actinic flux using the parameterization and our observations of the absorption properties of snow. We use the actinic flux parameterization to understand the sensitivity of the e-folding depth to ice grain size (effective grain radius), wavelength, solar zenith angle, and snowpack BC and nonBC concentrations at λ = 305 nm. Results from the parameterization suggest that actinic flux is significant at depths greater than 1.5 m in the snow. We evaluate the assumption made in previous studies (France et al., 2010, 2011, 2012; Wolff et al., 2002) that all NO_x produced in the snowpack will be ventilated to the overlying atmosphere by comparing the calculated depth-dependent lifetime of NO_x in the snowpack interstitial air against physical and chemical sinks. Using calculated actinic flux profiles and z_e, the parameterization can be easily integrated to calculate the snowpack actinic flux integrated over depth and wavelength to compute the total flux of NO_x from the snowpack, F_{NO_x}. Our calculated F_{NO_x} is compared to observations from inland sites in Antarctica and Greenland.

2 Methods

2.1 BC and nonBC Absorption from Filter Samples

The amount of absorption from BC and nonBC material in the snowpack must be known to calculate the actinic flux profile using our parameterization. In this study, the amount of BC and nonBC absorption is estimated from optical measurements of

ACPD
12, 15743–15799, 2012

impurities from the snow that have been collected on filters. Snow samples were collected for impurities in January 2004 at sites <0.5 to 11 km from Dome C Station in Antarctica, and in June 2007 at sites 20–40 km from Summit Station in Greenland (see Table 1). The snow samples were processed in the field. Each sample was melted and filtered through a 0.4 µm Nuclepore filter to extract the particulate material in the meltwater. A maximum of 10 % of the particulate matter in the snow sample is lost during filtering. The filters were transported back to the University of Washington where the optical properties of the filters were measured using the ISSW spectrophotometer as described in Grenfell et al. (2011). The ISSW spectrophotometer uses an integrating sphere and integrating sandwich technique to determine the absorption spectrum in units of optical depth, $T(\lambda)$ (dimensionless, e.g., $cm^2\,cm^{-2}$) from $\lambda = 300$–750 nm of particulate material on filters while removing losses from scattering by the filter and the collected aerosols (Grenfell et al., 2011).

The spectral absorption measured by the spectrophotometer for each filter is conventionally characterized by an Ångström exponent ($Å_{tot}$) associated with the absorption of total (BC + nonBC) impurities on each filter between two visible wavelengths (λ_1 and λ_2) according to the formula:

$$Å_{tot}(\lambda_1 \text{ to } \lambda_2) = \frac{\ln\left(\frac{T_{tot}(\lambda_1)}{T_{tot}(\lambda_2)}\right)}{\ln\left(\frac{\lambda_2}{\lambda_1}\right)}, \quad (1)$$

where the total optical depth, $T_{tot}(\lambda)$, describes the absorption of all the impurities on each filter at a given λ. A larger Ångström exponent indicates a greater absorption at shorter wavelengths (Fig. 1) resulting in a more brownish color for the sample.

Measured $Å_{tot}$ from $\lambda = 450$–600 nm is used together with the assumed values of $Å_{BC} = 1$ and $Å_{nonBC} = 5$ (Doherty et al., 2010, and references within) to determine the fraction of absorption from $\lambda = 450$–600 nm due to BC impurities ($f_{BC\_450–600}$) from the relation:

$$Å_{tot} = Å_{BC} \cdot f_{BC\_450–600}(\lambda_0) + Å_{nonBC}(1 - f_{BC\_450–600}(\lambda_0)), \quad (2)$$

ACPD
12, 15743–15799, 2012

where $\lambda_0 = 525$ nm. Since the absorption of radiation by BC is relatively constant with wavelength, $f_{BC\_450–600}$ is used to determine the fraction of absorption due to BC in the $\lambda = 650–700$ nm range ($f_{BC\_650–700}$), where BC is the dominant absorber of radiation (Grenfell et al., 2011). The maximum possible loading of BC on each filter (L_{maxBC}, $\mu g\,cm^{-2}$) for a given T_{tot} is calculated by assuming that all the absorption from $\lambda = 650–700$ nm is due to BC ($f_{BC\_650–700} = 1$) and calibrating the attenuation of transmitted light through the sample filter from $\lambda = 650–700$ nm against a calibration curve created with commercially produced BC as described in Grenfell et al. (2011).

The best estimate of the BC loading on each filter, L_{BC} ($\mu g\,cm^{-2}$) is determined by

$$L_{BC} = L_{maxBC} \cdot f_{BC\_650–700}, \quad (3)$$

The best estimate of BC concentration on a filter, C_{BC} ($ng\,C\,g^{-1}$), is calculated by multiplying L_{BC} by the exposed area of the filter, A (m^2), and dividing by the mass of meltwater filtered, M (g), as shown in Eq. (4):

$$C_{BC} = L_{BC} \cdot \frac{A}{M}, \quad (4)$$

The maximum concentration of BC on a filter, assuming BC is responsible for the total absorption in the 650–700 nm λ interval (C_{maxBC}), is calculated as shown in Eq. (5):

$$C_{maxBC} = L_{maxBC} \cdot \frac{A}{M}, \quad (5)$$

The total measured optical depth (T_{tot}) of each filter can be represented as the sum of the optical depth associated with BC material (T_{BC}) and the optical depth associated with nonBC material (T_{nonBC}) on each filter.

$$T_{tot}(\lambda) = T_{BC}(\lambda) + T_{nonBC}(\lambda), \quad (6)$$

T_{tot} is measured directly by the spectrophotometer. T_{BC} is calculated by multiplying L_{BC} by the mean average mass absorption efficiency of BC ($\beta_{BC} \sim 4.8\,m^2\,g_{BC}^{-1}$ at

ACPD
12, 15743–15799, 2012

λ = 675 nm), which is determined from Mie scattering calculations (Richard Brandt, personal communication, 2010). We calculate T_{nonBC} at various wavelengths using Eq. (7):

$$T_{\mathrm{nonBC}}(\lambda) = T_{\mathrm{nonBC}}(\lambda = 675\,\mathrm{nm}) \cdot \left(\frac{\lambda(\mathrm{nm})}{675}\right)^{-\text{Å}_{\mathrm{nonBC}}}. \quad (7)$$

Here, we assume $\text{Å}_{\mathrm{BC}} = 1$ and $\text{Å}_{\mathrm{nonBC}} = 5$ in the wavelength range λ = 298–412 nm to calculate the optical properties of BC and nonBC (including T_{BC} and T_{nonBC}) over that λ range and use the optical properties of BC and nonBC to calculate the actinic flux profile in the snow at South Pole, Summit, and Dome C. We discuss the sensitivity of this assumption in Sect. 3.6.

2.2 Inherent optical properties of BC, nonBC, and snow

In addition to the concentration of light-absorbing impurities or the amount of absorption due to the impurities in the snowpack, the inherent optical properties (IOPs) of the snowpack must also be known or estimated in order to calculate snowpack actinic flux. Inherent optical properties (IOPs), such as extinction coefficients (K_{ext}) and co-albedos of single scattering ($c\varpi$), describe the absorption, scattering, and extinction properties of a material (e.g., ice grains, BC, HULIS). K_{ext} (cm^{-1}) describes the amount of radiation removed from a beam of radiation traveling through a volume with a given cross-sectional area and length. $c\varpi$ (dimensionless, e.g., $\mathrm{cm\,cm}^{-1}$) describes the amount of absorption compared to extinction (scattering + absorption) in a medium. IOPs vary with λ for most materials. The effective IOPs for a given λ needed for a snow-

ACPD
12, 15743–15799, 2012

pack containing contaminants can be written:

$$K_{\mathrm{ext_{tot}}} = \sum_i K_{\mathrm{ext}_i}, \tag{8}$$

$$c\varpi_{\mathrm{eff}} = \frac{\sum_i c\varpi_i \cdot K_{\mathrm{ext}_i}}{K_{\mathrm{ext_{tot}}}}, \tag{9}$$

where $K_{\mathrm{ext_{tot}}}$ is the total extinction coefficient in the impurity-laden snowpack and K_{ext_i} represent the individual extinction coefficients for ice and impurities. Here, i indicates the components of the snowpack: ice and impurities (BC and nonBC). $c\varpi_{\mathrm{eff}}$ is the effective co-albedo of single scattering (1-single scattering albedo) of the impurity-laden snowpack and $c\varpi_i$ represents the individual co-albedos of single scattering for ice and impurities in the snow. The extinction coefficients and co-albedos of single scattering for snow, BC, and nonBC used in Eqs. (8) and (9) are given below.

The extinction coefficient for snow ($K_{\mathrm{ext_{snow}}}$) can be expressed as (Wiscombe and Warren, 1980):

$$K_{\mathrm{ext_{snow}}} = \frac{3Q_{\mathrm{ext}} \cdot \rho_{\mathrm{snow}}}{4r_{\mathrm{e}} \cdot \rho_{\mathrm{ice}}}, \tag{10}$$

where Q_{ext} is the extinction efficiency for snow grains (2.01 at 305 nm), ρ_{snow} is snow density (g cm^{-3}), ρ_{ice} is the density of ice (0.917 g cm^{-3}), and r_{e} is the radiation equivalent mean ice grain radius (μm) (Hansen and Travis, 1974). r_{e} is inversely proportional to specific surface area (SSA), where SSA = $3/(r_{\mathrm{e}} \cdot \rho_{\mathrm{ice}})$.

The extinction coefficient for BC ($K_{\mathrm{ext_{BC}}}$) in the snow can be calculated using the following equation:

$$K_{\mathrm{ext_{BC}}} = \frac{\beta_{\mathrm{BC}} \cdot C_{\mathrm{BC}} \cdot \rho_{\mathrm{snow}}}{c\varpi_{\mathrm{BC}}}, \tag{11}$$

ACPD
12, 15743–15799, 2012

where $c\varpi_{BC}$ is the single scattering co-albedo for BC (0.61 at 305 nm, Richard Brandt, personal communication, 2010). The wavelength dependence of the IOPs for both snow grains and soot particles are determined from Mie theory.

The extinction coefficient of nonBC material ($K_{ext_{nonBC}}$) is calculated using:

$$K_{ext_{nonBC}} = \frac{T_{nonBC} \cdot \left(\frac{A}{M}\right) \cdot \rho_{snow}}{c\varpi_{nonBC}}, \quad (12)$$

where $c\varpi_{nonBC}$ is the co-albedo of single-scattering for nonBC material. The contribution of scattering by BC and nonBC is insignificant because $K_{ext_{tot}}$ is dominated by snow grain scattering; therefore any value of $c\varpi_{nonBC}$ can be used in Eq. (12) (here, we use $c\varpi_{nonBC} = 1$). If additional absorbers are to be included, the attenuation coefficient can be easily developed from a direct extension of Eqs. (8) and (9) and appropriate modifications to equations of the form of Eq. (11).

2.3 Snowpack actinic flux parameterization

Once the IOPs are calculated for snow grains and impurities and combined to determine the effective IOPs of the snowpack at various λ, the effective IOPs are used to calculate vertical profiles of the actinic flux. The snowpack radiative transfer model used here is a 4-stream plane parallel radiative transfer model that uses the discrete ordinates method (DOM) with a δ-M transformation as described in Grenfell (1991). The 4-stream approximation provides better than 1 % numerical accuracy in albedo and absorptivity relative to exact high-order models for optical properties representative of snow (Wiscombe, 1977) and produces results identical to those from the DISORT model (Stamnes et al., 1988). We use this snowpack radiative transfer model (Grenfell, 1991) to develop a parameterization to calculate the depth-dependent actinic flux profile in snowpacks. The motivation to develop this parameterization is based on the need to include snowpack chemical processes in large scale models of the atmosphere in order to estimate the impact of these processes on regional scale nitrogen

ACPD
12, 15743–15799, 2012

and oxidant budgets. This parameterization is based on the δ-Eddington formulation (Wiscombe and Warren, 1980) modified by a correction factor from the 4-stream DOM model (Grenfell, 1991) and accounts for the spatio-temporal variations in the properties of the snowpack and ambient lighting conditions. New values of the optical properties of ice (Warren and Brandt, 2008) have been incorporated, which indicate much greater UV transmission in the snowpack than in previous work (Wolff et al., 2002). We vary r_e with depth in the modeled snowpack following observed vertical r_e profiles in snowpits near Dome C station (Gallet et al., 2011), but the vertical r_e profiles in this parameterization can easily be altered in order to calculate actinic flux profiles in a wide range of snow types. These equations retain the general capability to vary the properties of the snow to represent actinic flux accurately over a wide range of snow conditions present in Antarctica and Greenland, provided that the snow cover is deeper than three times z_e ($3z_e$). This parameterization is straightforward to implement into large scale models of the atmosphere.

For collimated incident radiation at the surface ($z = 0$)

$$\left[\frac{I_0(\lambda, z=0)}{F_{\text{inc}}(\lambda)}\right]_{\text{direct}} = \left[\frac{0.577+\mu_0}{0.577\cdot\mu_0}\right]\cdot \text{Corr}(\mu_0), \quad (13)$$

where $I_0(\lambda, z=0)_{\text{direct}}$ is the snowpack actinic flux from direct beam radiation at the surface, $F_{\text{inc}}(\lambda)_{\text{direct}}$ is the direct downwelling irradiance at the surface, μ_0 is the cosine of the solar zenith angle (θ), and Corr(μ_0) is a correction factor for θ (see Table 2). The magnitude of the correction factor is less than 6.4 % for all zenith angles except for $\theta = 85^\circ$, which is an angle not well represented by the δ-Eddington approximation, but for which solar radiation levels are very low.

Because the snowpack is such a strong volume scatterer in the UV (single scattering albedo >0.9999) the direct beam downwelling irradiance, if present, becomes negligible within 2 cm of the upper surface of a thick snowpack. Thus it is convenient to define a reference depth (z_{ref}) of 2 cm below which the radiation field is purely diffuse.

For $z \geq z_{\text{ref}}$, $I_0(\lambda, z)_{\text{direct}}$ for collimated incident radiation follows an exponential decay law that depends on the physical properties of the snowpack and the concentration of

ACPD
12, 15743–15799, 2012

impurities such as BC and nonBC as follows:

$$\left[\frac{I_0(\lambda, z \geq z_{\text{ref}})}{F_{\text{inc}}(\lambda)}\right]_{\text{direct}} = G(z_{\text{ref}}, \mu_0) \cdot e^{-0.60 \cdot Y \cdot (z - z_{\text{ref}})}, \quad (14)$$

where G is a factor designed to treat the non-exponential decay of radiation in the top 2 cm. G is calculated in Eq. (15):

$$G(z_{\text{ref}}, \mu_0) = 3(0.577 + \mu_0) \cdot e^{-0.60 \cdot Y \cdot z_{\text{ref}}} \cdot \text{Corr}(\mu_0), \quad (15)$$

and the attenuation coefficient for diffuse radiation (Y) is expressed as:

$$Y = (c\varpi_{\text{eff}})^{\frac{1}{2}} \cdot K_{\text{ext}_{\text{tot}}} = K_{\text{ext}_{\text{tot}}}{}^{\frac{1}{2}} \cdot [\sum_i c\varpi_i \cdot K_{\text{ext}_i}]^{\frac{1}{2}}, \quad (16)$$

For the diffuse component of the actinic flux, $I_0(\lambda, z)_{\text{diffuse}}$ follows an exponential decay law beginning from the snow surface ($z = 0$):

$$\left[\frac{I_0(\lambda, z)}{F_{\text{inc}}(\lambda)}\right]_{\text{diffuse}} = 3.831 \cdot e^{-0.60 \cdot Y \cdot z}, \quad (17)$$

Where $F_{\text{inc}}(\lambda)_{\text{diffuse}}$ is the diffuse downwelling irradiance at the surface. Because of strong Rayleigh scattering in the UV, there is a significant diffuse component to the incident radiation even for cloud free cases.

When both the direct and diffuse components of the downwelling irradiance are present, the combined (direct + diffuse) actinic flux $I_0(\lambda, z)$ at a given depth (z) and wavelength (λ) is calculated as:

$$I_0(\lambda, z) = \left\{\left[\frac{I_0(\lambda, z)}{F_{\text{inc}}(\lambda)}\right]_{\text{diffuse}} \cdot (f_{\text{dif}}) + \left[\frac{I_0(\lambda, z)}{F_{\text{inc}}(\lambda)}\right]_{\text{direct}} \cdot (1 - f_{\text{dif}})\right\} \cdot [F_{\text{inc}}(\lambda)]_{\text{tot}}, \quad (18)$$

where f_{dif} is the fraction of diffuse incident radiation compared to total (direct + diffuse) radiation and $F_{\text{inc}}(\lambda)_{\text{tot}}$ is the sum of the direct ($F_{\text{inc}}(\lambda)_{\text{direct}}$) and diffuse ($F_{\text{inc}}(\lambda)_{\text{diffuse}}$)

ACPD
12, 15743–15799, 2012

downwelling irradiance at the surface. Equation (18) can be integrated over depth and wavelength to calculate the total actinic flux ($II_0(\Delta\lambda_j, \Delta z_i)$) contributing to photochemical reactions (see Appendix).

We use the Fast-J radiative transfer program (Wild et al., 2000) in the GEOS-Chem global chemical transport model (http://www.geos-chem.org) (Bey et al., 2001) to calculate the diffuse and direct downwelling solar radiation at the surface at different locations in Greenland and Antarctica in seven wavelength bins between $\lambda = 289$ nm and $\lambda = 850$ nm. We specify a UV surface albedo of 0.996 in GEOS-Chem based on discrete ordinate method results (Grenfell, 1991). The above parameterization (Eq. 18) is used for sensitivity studies to examine which variables (e.g., BC, nonBC, r_e, θ) most strongly influence the actinic flux ($\lambda = 305$ nm) profile in the snowpack.

2.4 Calculating the depth dependent lifetime of NO_x in snowpack

Due to our calculated $3z_e > 1.5$ m in some locations (Sect. 3.3), we examine whether the NO_x produced via NO_3^- photolysis at depth will escape into the overlying atmosphere via diffusion and wind pumping before being re-oxidized to HNO_3. We define the escape lifetime (τ_{escape}) as the lifetime of NO_x in the snowpack interstitial air against transport to the overlying atmosphere via diffusion and wind pumping. The chemical lifetime ($\tau_{chemical}$) represents the lifetime of NO_x in the snowpack interstitial air against conversion to HNO_3, $BrONO_2$, and $IONO_2$ in the snowpack via the following reactions:

$$NO_2 + OH \rightarrow HNO_3, \quad \text{(R1)}$$

$$NO_2 + BrO \rightarrow BrONO_2, \quad \text{(R2)}$$

$$NO_2 + IO \rightarrow IONO_2, \quad \text{(R3)}$$

We determine the lifetime of NO_x with respect to escape (τ_{escape}) by calculating the lifetime of NO_x against diffusion ($\tau_{diffusion}$) and wind pumping ($\tau_{wind\ pumping}$) and adding

ACPD
12, 15743–15799, 2012

$\tau_{\text{diffusion}}$ and $\tau_{\text{wind pumping}}$ in parallel:

$$\tau_{\text{escape}} = \left(\frac{1}{\tau_{\text{diffusion}}} + \frac{1}{\tau_{\text{wind pumping}}} \right)^{-1}. \quad (19)$$

The characteristic time of NO_x for diffusion out of the snowpack is calculated according to Albert and Shultz (2002):

$$\tau_{\text{diffusion}} = \frac{z^2}{D_s}, \quad (20)$$

where z is snowpack depth and D_s, the diffusion coefficient of NO_x in snow, is defined (Albert and Shultz, 2002) as:

$$D_s = D_a \cdot \left(\frac{\Omega}{\xi^2} \right), \quad (21)$$

Here, D_a is the diffusion coefficient of NO_x in air ($0.14\,\text{cm}^2\,\text{s}^{-1}$) (Massman et al., 1998). We assume that D_a is independent of temperature in the top several meters of snowpack and find that this assumption is unimportant as diffusion is not the dominant escape process in the snowpack (Sect. 3.4). ξ is the tortuosity factor for aged snow ($1.3\,\text{cm}\,\text{cm}^{-1}$) (Pinzer et al., 2010). The porosity of snowpack (Ω) is defined in Albert and Shultz (2002):

$$\Omega = 1 - \rho_{\text{snow}} \cdot (\rho_{\text{ice}}^{-1}), \quad (22)$$

where ρ_{ice} is the density of ice ($0.92\,\text{g}\,\text{cm}^{-3}$) and ρ_{snow} is assumed constant with depth ($0.36\,\text{g}\,\text{cm}^{-3}$) (Albert and Shultz, 2002; Gallet et al., 2011; Grenfell et al., 1994). $\rho_{\text{snow}} = 0.36\,\text{g}\,\text{cm}^{-3}$ falls centrally within the range of measurements made in the top 2 m of snow at South Pole from Brandt and Warren (1997).

ACPD
12, 15743–15799, 2012

The characteristic escape time of NO_x (and other gaseous compounds in the snowpack) for wind pumping is calculated according to Waddington et al. (1996):

$$\tau_{\text{wind pumping}} = \frac{1}{C} \cdot \frac{\lambda_s}{h} \cdot \left[\frac{\mu/\rho_{\text{air}}}{U\lambda_s} \right] \cdot \frac{\Omega\lambda_s^2}{2\pi K} \cdot \frac{\lambda_s}{U} \cdot e^{\frac{2\pi z}{\lambda_s}}, \quad (23)$$

where, λ_s is sastrugi wavelength (cm), h is sastrugi height (cm), and U is horizontal windspeed at the surface ($m\,s^{-1}$) (see Table 3), ρ_{air} is air density calculated from the ideal gas law and the hypsometric equation using average summer air temperatures and the altitude of each station, μ is air viscosity (1.6×10^{-5} Pa·s), K is snow permeability (4×10^{-5} cm^2), and C is a constant of proportionality (~ 3) (Waddington et al., 1996).

The lifetime of NO_x in snowpack interstitial air against conversion to HNO_3, $BrONO_2$, and $IONO_2$ is calculated according to Seinfeld and Pandis (1998):

$$\tau_{NO_2+X} = (k_X[X])^{-1} \cdot \left(1 + \frac{[NO]}{[NO_2]}\right), \quad (24)$$

where X=OH, BrO, or IO and k_X is the corresponding rate constant ($cm^3\,molec^{-1}\,s^{-1}$) for R1–R3 from Sander et al. (2006).

The effective lifetime of NO_x against chemical conversion is calculated as:

$$\tau_{\text{chemical}} = \left(\frac{1}{\tau_{NO_2+OH}} + \frac{1}{\tau_{NO_2+BrO}} + \frac{1}{\tau_{NO_2+IO}} \right)^{-1}, \quad (25)$$

Formation of HNO_3(g) is considered a sink for snowpack NO_x because HNO_3(g) will not photolyze to NO_x prior to deposition onto the ice crystal surface. The lifetime of HNO_3(g) against photolysis (10–30 days in the tropics and longer in polar regions, Jacob et al., 1996; Tie et al., 2001) is much longer than its lifetime against deposition to the surface in polar regions (3.5–10 h) (Slusher et al., 2002; Wang et al., 2008).

ACPD
12, 15743–15799, 2012

Hydrolysis of $BrONO_2$ and $IONO_2$ on the surface of snow crystals to form HNO_3 and HOBr/HOI is also considered a sink for snowpack NO_x. However, $BrONO_2$ and $IONO_2$ can also photolyze to Br + NO_3 and I + NO_3, respectively (or less commonly, BrO + NO_2 and IO + NO_2, respectively).

The lifetime of $BrONO_2$ with respect to photolysis is calculated as:

$$\tau_{BrONO_2\_photolysis} = J_{BrONO_2}{}^{-1} = (I_0(\Delta\lambda_j, \Delta z_i) \cdot \phi_{BrONO_2} \cdot \sigma_{BrONO_2})^{-1} \quad (26)$$

where, $I_0(\Delta\lambda_j, \Delta z_i)$ is the total actinic flux in the λ = 289–500 nm bin at a specified depth in the snowpack, ϕ_{BrONO_2} is the quantum yield for the photolysis of $BrONO_2$ (0.15 for $\lambda > 300$ nm) (Sander et al., 2006), and σ_{BrONO_2} is the absorption cross section for $BrONO_2$ (Sander et al., 2006).

To calculate depth-dependent $\tau_{BrONO_2\_photolysis}$ in the snowpack, we use our calculated values of $I_0(\Delta\lambda_j, \Delta z_i)$ at λ = 289–500 nm (wavelengths relevant to $BrONO_2$ photolysis) (Burkeholder et al., 1995) from Eq. (18) using $\mu_0 = 60^\circ$ and r_e = 100 µm at local solar noon in January at Dome C and South Pole and in June at Summit. To estimate F_{inc} at $\lambda < 500$ nm in the λ = 412–850 nm range (consistent with Fast-J), we multiply the amount of direct radiation in the λ = 412–850 nm wavelength bin by the fraction [(500–412 nm)/(850–412 nm)]. This simplification is appropriate given that the solar flux is relatively constant throughout the λ = 412–850 nm range. The mean σ_{BrONO_2} in each wavelength bin is calculated by taking the average σ_{BrONO_2} within each bin from Burkholder et al. (1995). The photolysis rates are summed over the bins to create a depth-dependent $BrONO_2$ photolysis rate from λ = 289–500 nm.

The lifetime of $BrONO_2$ with respect to hydrolysis is calculated as:

$$\tau_{BrONO_2\_hydrolysis} = (k_{BrONO_2+H_2O(s)})^{-1}, \quad (27)$$

where,

$$k_{BrONO_2+H_2O(s)} = \left(\frac{r_e}{D_g} + \frac{4}{\upsilon\gamma}\right)^{-1} \cdot SA, \quad (28)$$

ACPD
12, 15743–15799, 2012

Here, $k_{BrONO_2+H_2O(s)}$ is the first order rate constant for uptake of $BrONO_2$ on the ice crystal surface (molecules cm^{-3} s^{-1}), r_e is the snow grain radius (0.01 cm), D_g is the gas-phase molecular diffusion coefficient of $BrONO_2$ in air (0.2 cm^2 s^{-1}), γ is the reaction probability (0.2) (Sander et al., 2006), υ is the mean molecular speed of $BrONO_2$ in the gas phase (3×10^4 cm s^{-1}), and SA is the corresponding snow grain surface area per unit volume of air, (177 cm^2 cm^{-3}) calculated in Eq. (29):

$$SA = \frac{3 \cdot \rho_{snow}}{r_e \cdot (\rho_{ice} - \rho_{snow})}. \quad (29)$$

Table 4 contains the values for the variables used to calculate $\tau_{chemical}$ (Eq. 25). Although the formation of $IONO_2$ may influence $\tau_{chemical}$, no measurements of IO have been made in polar continental regions so we assume [IO] = 0 at South Pole, Dome C, and Summit (and evaluate this assumption in Sect. 3.4). Whenever possible, we use observed concentrations of OH, BrO, NO, and NO_2 at the surface to calculate $\tau_{chemical}$. While there have been direct measurements of summertime boundary layer BrO at Summit (Liao et al., 2011; Stutz et al., 2011), there have been no direct measurements of boundary layer BrO at the South Pole and Dome C. To estimate the summertime average BrO concentrations where observations are not available, we use modeled BrO surface concentrations from Yang et al. (2005) and Yang (unpublished results, 2012).

We then calculate the OH, BrO, NO, and NO_2 vertical concentration profiles in the snowpack using two different approaches. The first approach assumes that chemical profiles are controlled by amount of radiation in the snowpack. In this approach we obtain concentration profiles of OH, BrO, NO, and NO_2 in the snowpack by scaling the observed or modeled surface concentrations by the calculated actinic flux from the surface to 200 cm depth at λ = 305 nm. The depth scaling factor is based on the assumption that OH, BrO, NO, and NO_2 are all produced through photochemical processes within the snowpack (Grannas et al., 2007 and references within). Two vertical chemical profiles are created for each station by using the direct radiation depth profile and the diffuse radiation depth profile to provide bounds as average surface conditions

ACPD
12, 15743–15799, 2012

will generally be a combination of both direct and diffuse downwelling radiation. For the second approach, we use modeled vertical chemical profiles in the snowpack for OH, BrO, NO, and NO_2 from Thomas et al. (2011). Using the profiles from this study we include effects of transport in the snow interstitial air, while the first approach only considers production rates and neglects transport within the snowpack column. For Antarctica, we scale the Summit profiles (Thomas et al., 2011) by surface observations and boundary layer model estimates of OH, BrO, NO, and NO_2 from South Pole (Davis et al., 2004; Mauldin et al., 2010; Yang et al., 2005, unpublished results), and Dome C (France et al., 2011; Frey et al., 2012; Yang et al., 2005, unpublished results). Using these relationships and observed, modeled, or assumed surface concentrations of OH, BrO, NO, and NO_2 at each station, we create a vertical profile of the concentration of these species in the snowpack at each station. Our scaled vertical chemical profiles at South Pole, Summit, and Dome C based upon the profiles in Thomas et al. (2011) indicate firn air NO_x concentrations on the order of 10^{-9} mol mol^{-1}, which is in good agreement with measured firn air NO_x concentrations at Dome C (Frey et al., 2012). For both approaches, we examine the sensitivity of the lifetime of NO_x with respect to chemical sinks using a range of summertime concentrations for each species at each location (see Table 4 for concentration ranges).

2.5 NO_x flux calculations

Nitrate photolysis in the snowpack is represented as (Warneck and Wurzinger, 1988):

$$NO_3^- + h\nu(+H^+) \rightarrow NO_2 + OH \quad \text{(R4)}$$

The flux of NO_x out of the snowpack from the photolysis of nitrate, F_{NO_x} (molecules cm^{-2} s^{-1}), is calculated via:

$$F_{NO_x} = \sigma_{NO_3^-}(\lambda) \cdot \phi_{NO_x}(T, \text{pH}) \cdot I_0(\Delta\lambda_j, \Delta z_i) \cdot [NO_3^-], \quad (30)$$

In Eq. (30), $\sigma_{NO_3^-}$ is the absorption cross section for nitrate photolysis (cm^2), ϕ_{NO_x} is the quantum yield for nitrate photolysis (unitless), $I_0(\Delta\lambda_j, \Delta z_i)$ is the depth-integrated total

ACPD
12, 15743–15799, 2012

actinic flux in a given wavelength bin (photons cm s^{-1}), and [NO_3^-] is the average nitrate concentration over the integration depth (molecules cm^{-3}). Please see the Appendix for calculation of $I_0(\Delta\lambda_j, \Delta z_i)$.

F_{NO_x} is calculated for local solar noon conditions in January at Dome C and South Pole and in June at Summit using $I_0(\Delta\lambda_j, \Delta z_i)$ calculated from Eq. (18) in the λ = 298–345 nm range and mean $\sigma_{NO_3^-}$ and ϕ_{NO_x} from Sander et al. (2006). The wavelength range from 298–345 nm encompasses four wavelength bins from the Fast-J program: 298–307, 307–312, 312–320, and 320–345 nm. We use the mean absorption cross sections in each wavelength bin. We use the average daily mean January temperatures at Dome C (243 K) (Frey et al., 2009) and South Pole (244 K) (Orvig, 1970) and June temperatures at Summit (257 K) (Steffen and Box, 2001) to calculate the temperature dependent quantum yield for NO_x (ϕ_{NO_x}) from Chu and Anastasio (2003). The monthly mean overhead ozone column abundance in GEOS-Chem for January is 293 DU at South Pole, 306 DU at Dome C and for June is 349 DU at Summit.

We choose a range of nitrate concentrations appropriate for polar snowpacks based upon observations in the top 1 m of snowpack at each location (Dibb et al., 2004, 2007, 2010; Frey et al., 2009). The upper 2 cm of snowpack in polar regions have considerably higher nitrate concentrations compared to depths below 2 cm in the snowpack and experience a sharp decay in concentration from the surface to 2 cm (Frey et al., 2009; Rothlisberger et al., 2000). Below 2 cm, [NO_3^-] decreases more gradually until concentrations oscillate (representing seasonality) around a relatively constant value. In this study, we calculate the flux of NO_x from the snowpack (F_{NO_x}) using a two layer approach ($z = 0 - z_{ref}$ and $z = z_{ref} - 3z_e$) and assume a constant snowpack [NO_3^-] below 2 cm.

It is thought that only nitrate in the quasi-liquid layer (QLL) is photolyzable (Boxe et al., 2005; Chu and Anastasio, 2003; Dubowski et al., 2001) while nitrate in the ice lattice remains intact. The fraction of total nitrate in the QLL is unknown. We estimate the amount of nitrate in the snowpack available for photolysis by calculating the fraction of nitrate dry deposition relative to total (dry + wet) deposition of nitrate at each location

ACPD
12, 15743–15799, 2012

using the GEOS-Chem global 3-D chemical transport model (http://www.geos-chem.org). Nitrate that is dry deposited to the snowpack will likely remain on the surface of the ice crystals and has a much greater chance for photolysis compared to nitrate that has been embedded in the ice crystal lattice via wet scavenging. The annual mean fraction of dry deposited nitrate to total nitrate deposited (wet + dry) is 0.73 at Summit and 1 at South Pole and Dome C, suggesting that the majority of nitrate in ice crystals is located in the QLL and is thus available for photolysis. This conclusion does not take into account possible migration of nitrate within an ice crystal.

3 Results and discussion

3.1 BC and nonBC impurity concentrations from the filtering of snow samples

Table 1 describes the location of each snow sample, the best estimate of the concentration of BC on the filter (C_{BC}), the estimated fraction of absorption in the λ = 650–700 nm and λ = 298–345 nm ranges due to nonBC impurities ($f_{nonBC\_650–700}$, $f_{nonBC\_298–345}$), and the Ångström exponent (Å) measured in the 450–600 nm λ range for each sample. In the snow samples collected near (<0.5 km) and away (11 km) from the Dome C station, the average C_{BC} is $2.1 \pm 1.3\,ng\,g^{-1}$ and $0.6 \pm 0.2\,ng\,g^{-1}$, respectively. In the snow samples collected greater than 20 km from the Summit station, the average C_{BC} is $1.4 \pm 0.3\,ng\,g^{-1}$. C_{BC} in snowpack near the station at Dome C is 1.5–3.5 times greater than C_{BC}in snowpacks away from the stations at Dome C and Summit, highlighting the influence of station activity on impurity levels in the local snowpack. C_{BC} in Greenland snow is roughly three times higher than C_{BC} in snow 11 km away from Dome C station. This combined with the low accumulation rate at Dome C ($3\,g\,cm^{-2}\,yr^{-1}$) (Rothlisberger et al., 2000) compared to Summit ($25\,g\,cm^{-2}\,yr^{-1}$) (Dibb and Fahnestock, 2004) highlights the higher concentration of pollutants in the Northern Hemisphere compared to the Southern Hemisphere.

ACPD
12, 15743–15799, 2012

Measured Ångström exponents for the particulate material on the filters fall between the values of Å = 1, considered representative of pure BC and Å = 5 for HULIS (Doherty et al., 2010), and are smaller than Å ~ 3.8 for dust (Zender et al., 2003), indicating there is a mixture of nonBC and BC impurities in both the snowpacks near and remote from the station. In the snow samples collected near the stations at Dome C and Summit, the Å of the impurities is slightly smaller (closer to Å = 1 for BC) and C_{BC} is higher compared to snow collected further away from the station, suggesting that the C_{BC} is more strongly impacted by station activities than C_{nonBC}. At Dome C, the average Å in the λ = 450–600 nm range is 2.3 ± 0.4 for snow sampled less than 0.5 km from the station and 2.9 ± 0.4 for snow sampled 11 km from the station. In Greenland, the average Å in the 450–600 nm λ range is 2.7 ± 0.3 for snow sampled greater than 20 km from the station. The similarity in the Ångström exponents at remote locations near Summit and Dome C suggests that the ratio of C_{BC} to C_{nonBC} and the type of nonBC material is also similar, even with the factor of 2 difference in C_{BC} at Summit and Dome C. $f_{nonBC\_650–700}$ ranges from 20–35 % and $f_{nonBC\_298–345}$ ranges from 86–89 %, highlighting the increased absorption of nonBC in the UV/near-vis λ region. The fraction of nonBC absorption in Dome C samples decreases as the station is approached, as C_{BC} values increase. Of all the snow samples collected, $f_{nonBC\_650–700}$ and $f_{nonBC\_298–345}$ are largest in samples collected greater than 20 km from Summit Station.

3.2 Sensitivity of snowpack actinic flux to variations in atmospheric conditions and snowpack radiative properties

Figure 2 compares the vertical actinic flux profile in the snowpack calculated according to Eq. (18) to the profile calculated using the full snowpack radiative transfer model (Grenfell, 1991) for a deep (depth >3 m) snowpack. For this comparison, we use typical remote Antarctica conditions at λ = 305 nm: r_e = 100 µm, ρ_{snow} = 0.36 g cm^{-3}, and C_{BC} = 0.3 ng g^{-1}. We assume C_{nonBC} = 0 ng g^{-1} for simplicity and assume a constant reference density with depth of 0.36 g cm^{-3}. The parameterization shows good

ACPD
12, 15743–15799, 2012

agreement (within 2 % in the top 150 cm and within 8 % from 150–500 cm) with the full snowpack radiative transfer model for the above scenario and additional scenarios using various combinations of snowpack and radiative properties (not shown).

Figure 3 illustrates the dependence of snowpack actinic flux on wavelength (λ), black carbon concentration (C_{BC}), snow grain effective radius (r_e) (Hansen and Travis, 1974), and solar zenith angle (θ). Snow density (ρ_{snow}) was also varied around a typical range, but the results are not shown in Fig. 3 because changes in ρ_{snow} do not influence the actinic flux profile significantly. Figure 3a shows that the z_e decreases with decreasing λ. The λ dependence is primarily due to the fact that nonBC material is assumed to absorb radiation more effectively at shorter wavelengths (e.g., Å $\sim$ 5). If only BC is present, the λ dependence is much smaller (not shown).

Figure 3b shows the strong dependence of z_e on C_{BC} and C_{nonBC} with the e-folding depth decreasing with increasing C_{BC} and C_{nonBC}. The range of C_{BC} in Fig. 3b (0.3–3 ng g^{-1}) represents the observed range of C_{BC} in Antarctica (Warren and Clarke, 1990; Warren et al., 2006). The snowpack actinic flux profile when C_{BC} = 0 is included for reference. In Fig. 3b, over 80 % of the absorption at λ = 305 nm is due to nonBC material.

Figure 3c shows the strong dependence of z_e on radiation-equivalent ice grain radius (r_e) with z_e values decreasing with decreasing r_e (r_e is assumed constant with depth). The decrease of z_e with decreasing r_e is due to the increased scattering that occurs as the number of grains per unit volume increases (see Eq. 10). The black curve in Fig. 3c is the snowpack actinic flux profile calculated when r_e is varied from 86 µm at z = 0 to 460 µm at z = 500 cm based on r_e measurements made near Dome C station by Gallet et al. (2011) that are linearly extrapolated below 50 cm. The average vertical r_e profile measured near Dome C station by Gallet et al. (2011) is applied to all snowpacks simulated in this study in absence of detailed vertical r_e profiles at South Pole and Summit, but we note that the vertical r_e profiles between these locations vary. Sensitivity studies reveal that BC and nonBC impurities in the snow influence z_e more significantly than differences in r_e profiles, as long as the snowpacks are not experiencing melt.

ACPD
12, 15743–15799, 2012

Figure 3d shows the influence of the solar zenith angle (θ) on z_e for the case of collimated incident radiation. In the top 2 cm (inset of Fig. 3d), where direct radiation is scattered and converted to diffuse radiation, θ influences both the amount of radiation as well as the slope of the actinic flux profile in the snowpack. At $\theta < 50^\circ$, the actinic flux increases with depth in the first 2 cm. This is because scattering by an individual snow particle is strongly in the forward direction increasing the penetration of the photons; more scattering events are needed to deflect the photons that have entered the snowpack at small solar zenith angles back to the atmosphere (Bohren and Barkstrom, 1972). Below 2 cm, where the radiation is entirely diffuse, the slopes of the actinic flux profiles are the same for all values of θ. The depth profile for purely diffuse incident radiation is purely exponential and corresponds closely to the profile for $\theta = 54^\circ$ under clear sky conditions.

The results shown in Fig. 3 suggest that for a given λ, impurity concentration (C_{BC} and C_{nonBC}) and radiation-equivalent mean ice grain radius (r_e) affect the actinic flux profile in snowpack most significantly. Due to the difficulty in measuring C_{nonBC} and its optical properties, the concentration and optical properties of nonBC material, such as HULIS, represent the largest uncertainty in calculations of snowpack actinic flux.

3.3 E-folding depth of actinic flux in the snowpack

Table 5 lists the z_e values for $\lambda = 305$ nm and $\lambda = 400$ nm for snow near the station at Dome C and South Pole and away from the station at Dome C, South Pole, and Summit calculated using Eq. (18) along with the observed C_{BC} at each location. We also include observed C_{BC} in South Pole snowpack; $C_{BC} = 3\,\mathrm{ng\,g^{-1}}$ was measured just downwind of the station and $C_{BC} = 0.3\,\mathrm{ng\,g^{-1}}$ was measured in the clean air sector (close to and upwind of the Atmospheric Research Observatory) (Warren and Clarke, 1990). We assume $f_{BC\_450–600}$ is similar at South Pole and Dome C because both stations are located high on the Antarctic plateau, which allows us to quantify the influence of nonBC material on UV/near-vis absorption at South Pole. In all cases, z_e is shallower at $\lambda = 305$ nm

ACPD
12, 15743–15799, 2012

than at $\lambda = 400$ nm due to the wavelength dependence of the inherent optical properties of nonBC material (see Fig. 1). In snowpacks with low impurity concentrations (remote, polar snowpacks), z_e is even deeper because as r_e increases with depth, scattering decreases, thus decreasing the probability of radiation absorption by impurities. z_e values are a factor of 1.8–3.5 larger at remote locations (>11 km) compared to locations near the stations (<0.5 km) because C_{BC} is 3.5–10 times greater in snow near the stations. Our calculated z_e values (12–14 cm) at Dome C assuming $r_e = 100\,\mu$m, $\lambda = 400$ nm, $C_{BC} = 3.3\,\mathrm{ng\,g^{-1}}$, and $\rho_{snow} = 0.35\,\mathrm{g\,cm^{-3}}$ compare well to the z_e values observed by France et al. (2011) (10–20 cm). For this comparison, $C_{BC} = 3.3\,\mathrm{ng\,g^{-1}}$ was chosen to match the measured values at this location (Warren et al., 2006), and $f_{BC\_450–600}$ from near-station snowpack at Dome C was used to calculate τ_{nonBC}.

3.4 The depth-dependent lifetime of NO_x in the snowpack

Figure 4 illustrates the depth-dependent lifetime of NO_x in the snowpack interstitial air against escape to the overlying atmosphere via diffusion ($\tau_{diffusion}$), wind pumping ($\tau_{wind\ pumping}$), and the combination of diffusion and windpumping (τ_{escape}) for a typical snowpack at Dome C. In Fig. 4, τ_{escape} ranges from 0 s at the surface, 11 min at 10 cm depth, and 7.4 days at 2 m depth. τ_{escape} at Dome C is dominated by diffusion in the top 10 cm, wind pumping from 10 to 40 cm, and diffusion below 40 cm. In the top 10 cm, diffusion is dominant because the distance to the free atmosphere is short; the distance approaches zero at the surface. From 10–40 cm wind pumping is dominant because the path that wind travels in the snow has a nonzero length as long as the surface topographic bumps have nonzero wavelength. Below 40 cm, diffusion is dominant because wind penetrates a finite distance into the snowpack. $\tau_{diffusion}$ and $\tau_{wind\ pumping}$ in Summit and South Pole snow exhibit the same general behavior (not shown), although the regions of dominance vary slightly between locations depending on the assumed summertime sastrugi dimensions and wind speeds. The lifetime of NO_x for diffusion from the snowpack is the same at Dome C, Summit, and South Pole,

ACPD
12, 15743–15799, 2012

but wind pumping is a more dominant ventilation process at South Pole and Summit than at Dome C because Summit and South Pole experience faster wind speeds and larger sastrugi wavelengths compared to Dome C. Variation of sastrugi dimensions (height and wavelength), wind speed, permeability, porosity, tortuosity, density, and the diffusion coefficient of NO_2 in snow around typical ranges for each station reveal that τ_{escape} is most sensitive to sastrugi dimensions (height and wavelength), wind speed, and permeability. Changes in porosity, tortuosity, density, and the diffusion coefficient of NO_2 in snowpack have a minimal impact on τ_{escape}. Decreasing the permeability decreases the importance of wind pumping in the top 2 m of the snow. Decreasing the sastrugi height and increasing the sastrugi wavelength also decreases the impact of windpumping in the top 2 m of the snow. Increasing the wind speed increases the impact of wind pumping at all depths in the snowpack.

Figure 5 shows the chemical lifetime of NO_x ($\tau_{chemical}$) in the snowpack against conversion to HNO_3 (τ_{NO_2+OH}) and $BrONO_2$(τ_{NO_2+BrO}). We assume that the formation of $BrONO_2$ represents a sink for NO_x because the calculated lifetime of $BrONO_2$ against hydrolysis onto snow grains (0.0006 s) is much shorter than the lifetime against photolysis (3–5 min) due to the large surface area of snow grains in the snowpack (Michalowski et al., 2000). Thus, we consider reactions R1-R3 to be sinks for NO_x in the snowpack. The vertical profiles of BrO, OH, NO, and NO_2 concentrations are determined using two different approaches described in Sect. 2.3 and are compared in Fig. 5. The dashed lines use observed concentrations of BrO, OH, NO, and NO_2 at the surface, scaled at depth to the actinic flux at $\lambda = 305$ nm using our actinic flux parameterization (Eq. 18) and measured snowpack optical properties in remote Dome C. The solid lines use concentration profiles of OH, BrO, NO, and NO_2 from Thomas et al. (2011) scaled to surface observations and model estimates of OH, BrO, NO, and NO_2 at Dome C (or South Pole when Dome C observations are not available) (Frey et al., 2012; Mauldin et al., 2010; Yang et al., 2005, unpublished results).

When the chemical concentrations are scaled to the actinic flux, the concentrations drop off exponentially with depth following the exponential decay of actinic flux in the

ACPD
12, 15743–15799, 2012

snowpack. When the chemical concentrations from Thomas et al. (2011) are used, the chemical profiles of OH, BrO, and NO increase from the surface, reach a maximum in concentration at 5–10 cm depth, then decay exponentially, following the decay of actinic flux in the snowpack. Efficient transport to the atmosphere above 5–10 cm depth combined with decreasing actinic flux with depth in the snowpack results in maximum OH, BrO, and NO concentrations at depths of 5–10 cm in the snowpack (Thomas et al., 2011). NO_2 remains relatively constant with depth in the snowpack because NO_2 has a longer lifetime than OH, BrO, and NO and its production rate and photolysis rate both decrease with depth. Also, NO to NO_2 conversions occur as NO_x is mixed downward out of the zone where photolysis occurs, leading to an accumulation of NO_2 in a photochemically inactive region.

At Dome C, South Pole (not shown), and Summit (not shown), the chemical lifetime of NO_x is mainly controlled by reactions with BrO when observed surface concentrations are scaled at depth to the actinic flux. $\tau_{chemical}$ increases more rapidly with depth below a depth of 10 cm using the modeled vertical profiles from Thomas et al. (2011) because their assumed z_e value (10 cm) is shallower than ours (18–22 cm). Although the chemical lifetimes vary dramatically at depth in the snowpack depending on the method used to calculate the chemical profiles in the snowpack, sensitivity studies reveal that τ_{escape} is always shorter than $\tau_{chemical}$.

Figure 6 shows the vertical profiles of $\tau_{chemical}$ and τ_{escape} in remote and near station snowpacks at Dome C, Summit, and South Pole calculated using average summertime values of snow density, snow permeability, sastrugi wavelength, sastrugi height, wind speed, and boundary layer [OH], [BrO], [NO], and [NO_2] each location. The chemical lifetimes in Fig. 6 were calculated by scaling surface NO, BrO, and OH concentrations by the actinic flux profile created with our actinic flux parameterization for snowpacks near the station (green curve) and snowpacks remote from the station (pink curve). We assume snowpack [NO_2] is constant with depth in the snowpack. The full range of expected values for each variable (snow density, snow permeability, sastrugi wavelength, sastrugi height, wind speed, [OH], [BrO], [NO], [NO_2]) in Eq. (19) (τ_{escape}) and Eq. (25)

ACPD
12, 15743–15799, 2012

($\tau_{chemical}$) are used in sensitivity studies. In all scenarios, τ_{escape} is always shorter than $\tau_{chemical}$, indicating that at all depths NO_x is efficiently ventilated to the overlying atmosphere via diffusion and wind pumping before being oxidized to HNO_3.

We have assumed [IO] = 0 in this study because IO that is produced in coastal regions due to biological activity quickly oxidizes and may deposit to coastal snow surfaces before being transported inland. However, if we assume IO concentrations are equal to the base-case BrO concentrations used in this study we find that our results are not changed. We find that the conversion of NO_2 to $BrONO_2$ and $IONO_2$ are equally dominant when concentrations of IO and BrO are equivalent due to similar reaction rate constants. The chemical concentrations of BrO, IO, and OH in the snowpack are highly uncertain, but are thought to be on the order of 10^{-12} mol mol^{-1} in the snowpack (Thomas et al., 2011). However, Frieß et al. (2010) observed IO concentrations at Neumayer on the order of 10^{-9} mol mol^{-1} while surface atmosphere observations were on the order of 10^{-12} mol mol^{-1}. If we use snowpack BrO and IO concentrations on the order of 10^{-9} mol mol^{-1}, we find that NO_x is not efficiently ventilated to the atmosphere at Dome C, South Pole, and Summit snowpacks. In this scenario, NO_x produced through photodenitrification would convert to HNO_3 before escaping to the atmosphere at all depths. If we use snowpack BrO, IO, and OH concentrations of 10^{-11} mol mol^{-1} levels, we find that NO_x is efficiently ventilated to the atmosphere in all snowpacks except those in remote Summit and Dome C snowpacks. In these remote snowpacks, below 10 cm at Summit and 30 cm at Dome C, NO_x would be converted to HNO_3 in the snowpack faster than ventilated to the overlying atmosphere, although radiation is still available for photochemical production of NO_x below these depths.

3.5 Results of NO_x flux calculations

Table 6 shows the results of our calculated flux of NO_x from the snowpack to the overlying atmosphere, F_{NO_x}, using observed nitrate concentrations scaled to the fraction of dry deposited nitrate at each location as described in Sect. 2.5. The range of F_{NO_x} represents calculations using the full range of observed nitrate concentrations (Dibb

ACPD
12, 15743–15799, 2012

et al., 2004, 2007; Frey et al., 2009). Our calculations are compared to observations in the vicinity (<5 km) of each station. The NO_x fluxes calculated in this study are in good agreement with observed NO_x fluxes measured near the station at South Pole (Davis et al., 2004; Oncley et al., 2004) and calculated NO_x fluxes near the station at Dome C (France et al., 2011). The NO_x flux modeled by France et al. (2011) is at the high end of NO_x flux observations at Dome C (Frey, personal communication, 2011).

The vertical r_e profile is the same for all snowpacks considered in the study, therefore the concentration of impurities and NO_3^- in the snow influence our calculated flux of NO_x from the snowpack most significantly. The NO_x fluxes from snowpacks greater than 11 km from the station are 1.4–2.4 times larger than the NO_x fluxes from snowpacks near the stations at South Pole and Dome C because near-station snowpacks have higher concentrations of impurities, resulting in shallower e-folding depths in near-station snowpacks. Shallower z_e values near stations confine photodenitrification to a shallower layer, resulting in less NO_x produced (and transported to the atmosphere) compared to remote snowpacks. Here we assume that the snowpack $[NO_3^-]$ at South Pole, Dome C, and Summit is the same for each station regardless of distance from the station. The range of F_{NO_x} at each location represents the difference between minimum and maximum observed snowpack $[NO_3^-]$.

The contributions of the top 2 cm of snowpack to the total F_{NO_x} vary between stations (24–68 %), but are generally greater in snowpacks near the stations because of shallower e-folding depths of actinic flux. We expect the photodenitrification occurring in the top 2 cm of snow to significantly influence F_{NO_x} because $I_0(\lambda, z)$ and $[NO_3^-]$ are greatest in that layer. Although the snowpack $[NO_3^-]$ is roughly 3 times higher in the top 2 cm at South Pole compared to Dome C and Summit, Summit has the highest snowpack $[NO_3^-]$ below 2 cm and therefore yields the largest flux of NO_x. Although remote South Pole snowpack has lower $[NO_3^-]$ compared to Summit, remote South Pole snowpack yields the second highest F_{NO_x} because it has the largest e-folding depth due to low impurity concentrations. The snowpack $[NO_3^-]$ and the e-folding depth of actinic flux influence F_{NO_x} comparably, which can lead to compensating effects. For example, the

ACPD
12, 15743–15799, 2012

minimum F_{NO_x} from snowpacks near the stations at South Pole and Dome C are similar because South Pole has higher $[NO_3^-]$ but Dome C has a larger e-folding depth. But in general, the highest F_{NO_x} results from high snowpack $[NO_3^-]$ and large e-folding depths.

3.6 Sensitivity of nonBC absorption on results

The absorption spectrum of nonBC is uncertain (Doherty et al., 2010 and references within), and in this study we have chosen a value of $Å_{nonBC} = 5$ over the λ range 289–850 nm. To examine the sensitivity of this assumption on z_e and F_{NO_x} near and far from the stations at Dome C, Summit, and South Pole, we linearly extrapolate Eq. (7) over the UV wavelengths relative to photochemistry (λ = 289–345 nm) instead of assuming $Å_{nonBC} = 5$ over that λ range. We continue to assume $Å_{nonBC} = 5$ at λ longer than 345 nm. We find that linear extrapolation of Eq. (7) leads to smaller optical depths of nonBC, T_{nonBC}, indicating less absorption of UV radiation due to nonBC material in the snowpack compared to when we assume that $Å_{nonBC} = 5$ in the UV. However, the nonBC absorption is still dominant over BC absorption in the UV. Less absorption of UV radiation by nonBC material increases the e-folding depth at λ = 305 nm by 3–5 cm at all locations except remote South Pole, where the e-folding depth is increased by 10 cm. F_{NO_x} is increased by a factor of 1.13–1.23 depending on location.

For the typical snowpack chemical concentrations of BrO, OH, NO, and NO_2 used in this study we find that τ_{escape} is still shorter than $\tau_{chemical}$ at all locations, indicating that all NO_x produced in in the interstitial air is efficiently ventilated to the atmosphere when T_{nonBC} is extrapolated linearly in the UV λ range. However, $\tau_{chemical}$ becomes shorter than τ_{escape} at depths above $3z_e$ if the concentrations of BrO are increased by a factor of 4 at each location, suggesting that the NO_x produced below the depth where $\tau_{chemical}$ is shorter than τ_{escape} will be converted to HNO_3 before escaping to the atmosphere. When T_{nonBC} is determined by linear extrapolation in the UV instead of assuming $Å_{nonBC} = 5$, z_e is greater at $\lambda < 400$ nm because less UV radiation is absorbed by nonBC material. Since we have scaled the concentrations of BrO, IO, and OH by

ACPD
12, 15743–15799, 2012

the actinic flux in the snow, their concentrations are higher if less radiation is absorbed by nonBC material.

$\tau_{chemical}$ becomes shorter than τ_{escape} at depths above $3z_e$ either because concentrations of BrO, IO, and OH are increased to 10^{-11} mol mol^{-1} levels when $Å_{nonBC} = 5$ in the UV λ range or concentrations of BrO are increased by a factor of 4 when T_{nonBC} is linearly extrapolated in the UV λ range. In either case, the NO_x flux can be calculated by integrating the actinic flux from the surface to the depth where $\tau_{chemical}$ becomes shorter than τ_{escape}, instead of integrating to $z = 3z_e$. When $\tau_{chemical}$ and τ_{escape} are comparable in magnitude, sastrugi dimensions and wind speeds are important along with chemical concentrations in determining the fate of snowpack NO_x. Ranges of these variables (see Tables 3 and 4) should be used to determine the error bars associated with the depth that actinic flux must be integrated over to calculate the flux of NO_x from the snowpack.

4 Conclusions

Observations of the absorption properties of black carbon and non-black-carbon material (e.g., brown carbon, dust, organics) in snow collected near Dome C, Antarctica and Summit, Greenland show that near-station activities enhance the concentration of absorbing impurities by a factor of at least 2–3, and that the concentrations of absorbing impurities are a factor of 2.5–5 higher at remote locations in Greenland compared to remote locations in east Antarctica. The Ångström exponents associated with the absorption of particulate matter in snow range from 2.3–3 and indicate a combination of black carbon and non-black-carbon material in all snow sampled, the latter of which provides the dominant contribution to absorption of UV radiation in the snowpack. We find that absorption of radiation by nonBC is dominant over BC in the UV even if the optical depth for nonBC is determined by linear extrapolation rather than assuming an Ångström exponent of 5 in the UV. Our observations of absorption due to

ACPD
12, 15743–15799, 2012

BC and nonBC in snowpack at Dome C, Summit, and South Pole are incorporated into a snowpack actinic flux parameterization.

The parameterization is used to calculate depth-dependent actinic flux profiles in snowpack and is based upon a 4-stream, plane parallel snowpack radiative transfer model with a δ-M approximation (Grenfell, 1991). This parameterization is broadly applicable and allows straightforward inclusion of snowpack properties and impurity types and concentrations. It can be easily implemented into large scale models and represents spatio-temporal variations in solar zenith angle, wavelength, radiation-equivalent ice grain radius, snow density, and impurity concentration. The parameterization was used to calculate actinic flux profiles in snowpack for specific case studies near the stations at Dome C and South Pole and in remote Dome C, South Pole, and Summit. In the UV/near-vis region (the region relevant for photochemistry), the e-folding depth of actinic flux (z_e) is strongly dependent on impurity concentrations (BC and nonBC) and radiation equivalent mean ice grain radius (r_e). z_e decreases with increasing impurity concentration and increases with increasing r_e. Our calculated z_e values range from 8–62 cm between wavelengths of λ = 305–400 nm; z_e decreases with decreasing wavelength due to the wavelength dependence of nonBC absorption. Using measured BC concentrations from Warren et al. (2006) near the station at Dome C, Antarctica, our calculated z_e values of 12–14 cm near the station at Dome C agrees well with the z_e calculated by France et al. (2011) using observations of irradiance in snowpacks near Dome C station.

Our results from the parameterization suggest that UV/near-vis radiation is significant at depths greater than 1.5 m in the snowpack, which implies that photodenitrification can occur and produce NO_x at those depths. We calculate the depth dependent lifetime of NO_x in the snowpack for ventilation to the overlying atmosphere by diffusion and windpumping (τ_{escape}) and chemical sinks by reaction of NO_2 with OH and BrO ($\tau_{chemical}$). Comparison of the vertical profiles of τ_{escape} and $\tau_{chemical}$ reveals that NO_x is efficiently ventilated to the overlying atmosphere at all depths in the snowpack. This result is sensitive to the concentrations of BrO; if $\tau_{chemical}$ becomes shorter than τ_{escape}

ACPD
12, 15743–15799, 2012

at a depth above $3z_e$ due to an increase in BrO, the actinic flux must be integrated to that depth rather than to $3z_e$ when calculating the flux of NO_x from the snowpack, F_{NO_x}.

Our calculated F_{NO_x} near Dome C, South Pole, and Summit range from 3.2×10^8–2.8×10^9 molecules cm^{-2} s^{-1}. Calculated NO_x fluxes in snowpack near stations are a factor of 1.4–2.4 smaller than >11 km away from the stations due to the impact of absorbing impurity concentrations from local contamination on the e-folding depth of the actinic flux in snowpack. Observations of NO_x fluxes near stations are likely underestimating the amount of NO_x emitted from the snowpack in remote locations by a similar factor of 1.4–2.4.

Appendix A

NO_x flux calculation

The flux of NO_x from the snowpack (F_{NO_x}) is calculated for two distinct layers in the snowpack: from the surface ($z = 0$) to z_{ref} (2 cm) and from z_{ref} to three times the e-folding depth ($3z_e$) of actinic flux in snow. These layers are separate because the decay of radiation with depth is in general non-exponential from 0–2 cm and exponential below 2 cm depth. Also, there are significant differences in the vertical profile of snowpack [NO_3^-] in the two layers (see Sect. 2.5). The total downwelling irradiance at the snowpack surface is calculated for multiple wavelength bins by the Fast-J radiative transfer program (Wild et al., 2000) with the surface albedo specified to be consistent with our snowpack calculations (0.996). Summations over each λ bin are carried out after depth integrations to insure that the λ dependence of the e-folding depths are properly included.

In the λ bin ($\lambda_{j+1} - \lambda_j = \Delta\lambda_j$), $I_0(\Delta\lambda_j, z)$ is first calculated at each centimeter in the snowpack from the surface ($z = 0$ cm) to a depth of 3 times the e-folding depth of actinic flux in snow ($3z_e$). Once $I_0(\Delta\lambda_j, z)$ has been calculated at each centimeter,

ACPD
12, 15743–15799, 2012

the total (integrated) actinic flux, $II_0(\Delta\lambda_j, \Delta z_i)$, is calculated in a 2 cm interval from $z = 0$ to z_{ref} and 1 cm intervals from $z = z_{\text{ref}}$ to $3z_e$ ($z_{i+1} - z_i = \Delta z_i$). Intervals of 1–2 cm are used because IOPs ($c\varpi_{\text{eff}}$ and $K_{\text{ext}_{\text{tot}}}$) vary with depth due to the dependence of grain radius on depth. In each depth interval and wavelength bin, an average Y value ($\overline{Y}_{ij} = \overline{c\varpi_{\text{eff}}^{\frac{1}{2}}}(\Delta\lambda_j, \Delta z_i) \cdot \overline{K_{\text{ext}_{\text{tot}}}}(\Delta\lambda_j, \Delta z_i)$) is used, which uses average values of $K_{\text{ext}_{\text{tot}}}$ and $c\varpi_{\text{eff}}$ over $\Delta\lambda_j$ and each Δz_i. From $z_1 = 0$ to $z_2 = z_{\text{ref}}$, $I_0(\Delta\lambda_j, z)$ is numerically integrated over each λ bin ($\Delta\lambda_j$) in the depth interval ($\Delta z_1 = z_2 - z_1$) using the trapezoid rule.

$$II_0\left(\Delta\lambda_j, 0\,\text{cm to } 2\,\text{cm}\right) = \frac{I_0\left(\Delta\lambda_j, z_1\right) + I_0\left(\Delta\lambda_j, z_2\right)}{2} \cdot \Delta z_1 \tag{A1}$$

Below z_{ref}, $I_0(\Delta\lambda_j, z)$ is analytically integrated over 1 cm intervals (Δz_i).

$$II_0\left(\Delta\lambda_j, \Delta z_i\right) = I_0\left(\Delta\lambda_j, z_i\right) \cdot \int_{z_i}^{z_{i+1}} \mathrm{e}^{-\bar{\mathrm{Y}} \cdot z'} dz', \tag{A2}$$

When evaluated, Eq. (A2) becomes:

$$II_0\left(\Delta\lambda_j, \Delta z_i\right) = I_0(\Delta\lambda_j, z_i) \cdot \left\{ \frac{(e^{-\bar{\mathrm{Y}} \cdot z_i} - e^{-\bar{\mathrm{Y}} \cdot z_{i+1}})}{\bar{\mathrm{Y}}} \right\}, \tag{A3}$$

Values of $II_0\left(\Delta\lambda_j, \Delta z_i\right)$ calculated in each depth interval (Δz_i) in the $z = z_{\text{ref}}$ to $3z_e$ layer are summed in each λ bin ($\Delta\lambda_j$).

$$II_0\left(\Delta\lambda_j, 2\,\text{cm to } z_{3\text{efolds}}\right) = \sum_{i=2}^{i=z_{3\text{efolds}}} II_0\left(\Delta\lambda_j, \Delta z_i\right), \tag{A4}$$

ACPD
12, 15743–15799, 2012

The total flux of NO_x from the snowpack from the layer $z = 0$ to $3z_e$ in each λ bin, $F_{NO_x}(\Delta\lambda_j, 0\,\text{cm to } z_{3efolds})$, is calculated in Eq. (A5):

$$F_{NO_x}\left(\Delta\lambda_j, 0\,\text{cm to } z_{3efolds}\right) = \bar{\phi}\left(\Delta\lambda_j\right)\cdot\bar{\sigma}\left(\Delta\lambda_j\right)\cdot\left(\overline{\left[NO_3^-\right]}_{\Delta z_1}\cdot I_0\left(\Delta\lambda_j, 0\,\text{cm to } 2\,\text{cm}\right) + \overline{\left[NO_3^-\right]}_{\Delta z_2 \text{ to } \Delta z_{3efolds}}\cdot I_0\left(\Delta\lambda_j, 2\,\text{cm to } z_{3efolds}\right)\right), \quad \text{(A5)}$$

where $\bar{\phi}\left(\Delta\lambda_j\right)$ is the average quantum yield and $\bar{\sigma}\left(\Delta\lambda_j\right)$ is the average absorption cross-section in the wavelength bin, $\Delta\lambda_j$. $\overline{\left[NO_3^-\right]}_{\Delta z_1}$ is the average snowpack nitrate concentration in the layer from $z = 0$ to z_{ref} and $\overline{\left[NO_3^-\right]}_{\Delta z_2 \text{ to } \Delta z_{3efolds}}$ is the average snowpack nitrate concentration in the layer from $z = z_{ref}$ to $3z_e$.

The total flux of NO_x (F_{NO_x}) from the surface snowpack associated with all λ relevant for photodenitrification ($\lambda = 298$–345 nm) is calculated by summing the total depth-integrated flux of NO_x from the snowpack in each λ bin. Here, 4 λ bins are used to calculate F_{NO_x} ($N_\lambda = 4$).

$$F_{NO_x} = \sum_{j=1}^{j=N_\lambda} F_{NO_x}\left(\Delta\lambda_j, 0\,\text{cm to } z_{3efolds}\right) \quad \text{(A6)}$$

Acknowledgements. Funding for this project is provided by NSF ANT 0944537 and EPA STAR graduate fellowship to M. C. Zatko. Stephen Warren collected and filtered the samples at Dome C. Lora Koenig collected the snow samples at Summit; Stephen Warren melted and filtered them. Stephen Warren and Delphine Six provided the measurements of sastrugi dimensions at Dome C. We thank Stephen Warren, Eric Sofen, Paul Hezel, and Lei Geng for comments on the draft manuscript. We thank Oliver Wild for helping us to better understand the Fast-J algorithm and Eric Wolff for his generous advice during the initial stages of this project. We thank Ed Waddington for insightful discussions about transport processes in the snow, Joel Thornton for helpful discussions about $BrONO_2$ hydrolysis in the snow, and Charlie Zender for information about the optical properties of dust.

ACPD
12, 15743–15799, 2012

References

Albert, M. R. and Hawley, R. L.: Seasonal changes in snow surface roughness characteristics at Summit, Greenland: implications for snow and firn ventilation, Ann. Glaciol., 35, 510–514, 2002.

Albert, M. R. and Shultz, E. F.: Snow and firn properties and air-snow transport processes at Summit, Greenland, Atmos. Environ., 36, 2789–2797, 2002.

Aristidi, E., Agabi, K., Azouit, M., Fossat, E., Vernin, J., Travouillion, T., Lawrence, J. S., Meyer, C., Storey, J. W. V., Halter, B., Roth, W. L., and Walden, V.: An analysis of temperatures and wind speeds above Dome C, Antarctica, Astron. Astrophys., 430, 739–746, 2005.

Askebjer, P., Barwick, S. W., Bergstrom, L., Bouchta, A., Carius, S., Dalberg, E., Engel, K., Erlandsson, B., Goobar, A., Gray, L., Hallgren, A., Halzen, F., Heukenkamp, H., Hulth, P. O., Hundertmark, S., Jacobsen, J., Karie, A., Kandhadai, V., Liubarsky, I., Lowder, D., Miller, T., Mock, P., Morse, R. M., Porrata, R., Price, P. B., Richards, A., Rubinstein, H., Schenider, E., Spiering, C., Streicher, O., Sun, Q., Thon, T., Tilav, S., Wischnewski, R., Walck, C., and Yodh, G. B.: Optical properties of deep ice at the South Pole: absorption, Appl. Optics, 36, 4168–4180, 1997a.

Askebjer, P., Barwick, S. W., Bergstrom, L., Bouchta, A., Carius, S., Dalberg, E., Engel, K., Erlandsson, B., Goobar, A., Gray, L., Hallgren, A., Halzen, F., Heukenkamp, H., Hulth, P. O., Hundertmark, S., Jacobsen, J., Karie, A., Kandhadai, V., Liubarsky, I., Lowder, D., Miller, T., Mock, P., Morse, R. M., Porrata, R., Price, P. B., Richards, A., Rubinstein, H., Schenider, E., Spiering, C., Streicher, O., Sun, Q., Thon, T., Tilav, S., Wischnewski, R., Walck, C., and Yodh, G. B.: UV and optical light transmission properties in deep ice at the South Pole, Geophys. Res. Lett., 24, 1355–1358, 1997b.

Beine, H. J., Honrath, R. E., Domine, F., Simpson, W. R., and Fuentes, J. D.: NO_x during background and ozone depletion periods at Alert: fluxes above the snow surface, J. Geophys. Res., 107, 4584 pp., doi:10.1029/2002/JD002082, 2002.

Bey, I., Jacob, D. J., Yantosca, R. M., Logan, J. A., Field, B. D., Fiore, A. M., Li, Q., Liu, H. Y., Mickley, L. J., and Schultz, M. G.: Global modeling of tropospheric chemistry with assimilated meteorology: model description and evaluation, J. Geophys. Res., 106, 23073–23095, 2001.

ACPD
12, 15743–15799, 2012

Beyersdorf, A. J., Blake, N. J., Swanson, A. L., Meinardi, S., Dibb, J. E., Sjostedt, S., Huey, G., Lefer, B., Rowland, S. F., and Blake, D. R.: Hydroxyl concentrations estimates in the sunlit snowpack at Summit, Greenland, Atmos. Environ., 41, 5101–5109, 2007.

Blunier, T., Gregoire, F. L., Jacobi, H.-W., and Quansah, E.: Isotopic view on nitrate loss in Antarctic surface snow, Geophys. Res. Lett., 32, L13501, doi:10.1029/2005GL023011, 2005.

Bohren, C. F. and Barkstrom, B. R.: Theory of the optical properties of snow, J. Geophys. Res., 79, 4527–4535, doi:10.1029/JC079i030p04527, 1974.

Boxe, C. S., Colussi, A. J., Hoffmann, M. R., Murphy, J. G., Wooldridge, P. J., Bertram, T. H., and Cohen, R. C.: Photochemical production and release of gaseous NO_2 from nitrate-doped water ice, J. Phys. Chem., 109, 8520–8525, 2005.

Brandt, R. E. and Warren, S. G.: Temperature measurements and heat transfer in near-surface snow at the South Pole, J. Glaciol., 43, 144, 339–351, 1997.

Burkholder, J. B., Ravishankara, A. R., and Solomon, S.: UV/visible and IR absorption cross sections of $BrONO_2$, J. Geophys. Res., 100, 16793–16800, 1995.

Chen, G., Huey, L. G., Crawford, J. H., Olson, J. R., Hutterli, M. A., Sjostedt, S., Tanner, D., Dibb, J., Lefer, B., Blake, N., Davis, D., and Stohl, A.: An assesment of the polar HO_x photochemical budget based on 2003 Summit Greenland field observations, Atmos. Environ., 41, 7806–7820, 2007.

Chu, L. and Anastastio. C.: Quantum yields of hydroxyl radicals and nitrogen dioxide from the photolysis of nitrate on ice, J. Phys. Chem., 107, 9594–9602, 2003.

Cotter, E. S. N., Jones, A. E., Wolff, E. W., and Bauguitte, S. J.-B.: What controls photochemical NO and NO_2 production from Antarctic snow? Laboratory investigation assessing the wavelength and temperature dependence, J. Geophys. Res., 108, 4147, doi:10.1029/2002JD002602, 2003.

Davis, D., Nowak, J. B., Chen, G., Buhr, M., Arimoto, R., Hogan, A., Eisele, F., Mauldin, L., Tanner, D., Shetter, R., Lefer, B., and McMurry, P.: Unexpected high levels of NO observed at South Pole, Geophys. Res. Lett., 28, 3625–3628, 2001.

Davis, D., Chen, G., Buhr, M., Crawford, J., Lenschow, D., Lefer, B., Shetter, R., Eisele, F., Mauldin, L., and Hogan, A.: South Pole NO_x chemistry: an assessment of factors controlling variability and absolute levels, Atmos. Environ., 38, 5375–5388, 2004.

Davis, D. D., Seelig, J., Huey, G., Crawford, J., Chen, G., Wang, Y., Buhr, M., Helmig, D., Neff, W., Blake, D., Arimoto, R., and Eisele, F.: A reassessment of Antarctic plateau reactive

ACPD
12, 15743–15799, 2012

nitrogen based on ANTCI 2003 airborne and ground based measurements, Atmos. Environ., 42, 2831–2848, doi:10.1016/j.atmosenv.2007.07.039, 2008.
Dibb, J. E., Arsenault, M., Peterson, M. C., and Honrath, R. E.: Fast nitrogen oxide photochemistry in summer, Greenland snow, Atmos. Environ., 36, 2501–2511, 2002.
Dibb, J. E., Huey, G. L., Slusher, D. L., and Tanner, D. J.: Soluble reactive nitrogen oxides at South Pole during ISCAT 2000, Atmos. Environ., 38, 5399–5409, 2004.
Dibb, J. E. and Fahnestock, M.: Snow accumulation, surface height change, and firn densification at Summit, Greenland: insights from 2 yr of in situ observation, J. Geophys. Res., 109, D24113, doi:10.1029/2003JD004300, 2004.
Dibb, J. E., Whitlow, S. I., and Arsenault, M.: Seasonal variations in the soluble ion content of snow at Summit, Greenland: constraints from three years of daily surface snow samples, Atmos. Environ., 41, 5007–5019, 2007.
Dibb, J. E., Ziemba, L. D., Luxford, J., and Beckman, P.: Bromide and other ions in the snow, firn air, and atmospheric boundary layer at Summit during GSHOX, Atmos. Chem. Phys., 10, 9931–9942, doi:10.5194/acp-10-9931-2010, 2010.
Doherty, S. J., Warren, S. G., Grenfell, T. C., Clarke, A. D., and Brandt, R. E.: Light-absorbing impurities in Arctic snow, Atmos. Chem. Phys., 10, 11647–11680, doi:10.5194/acp-10-11647-2010, 2010.
Domine, F. and Shepson, P. B.: Air-snow interactions and atmospheric chemistry, Science, 297, 1506–1510, 2002.
Dubowski, Y., Colussi, A. J., and Hoffmann, M. R.: Nitrogen dioxide release in the 302 nm band photolysis of spray-frozen aqueous nitrate solutions, atmospheric implications, J. Phys. Chem. A, 105, 4928–4932, 2001.
France, J. L., King, M. D., and Lee-Taylor, J.: The importance of considering depth-resolved photochemistry in snow: a radiative-transfer study of NO_2 and OH production in Ny-Ålesund (Svalbard) snowpacks, J. Glaciol., 56, 655–663, 2010.
France, J. L., King, M. D., Frey, M. M., Erbland, J., Picard, G., Preunkert, S., MacArthur, A., and Savarino, J.: Snow optical properties at Dome C (Concordia), Antarctica; implications for snow emissions and snow chemistry of reactive nitrogen, Atmos. Chem. Phys., 11, 9787–9801, doi:10.5194/acp-11-9787-2011, 2011.
France, J. L., Reay, H. J., King, M. D., Voisin, D., Jacobi, H.-W., Domine, F., Beine, H. J., Anastasio, C., MacArthur, A., and Lee-Taylor, J.: Hydroxyl radical and NO_x production rates, black carbon concentrations and light-absorbing impurities in snow from field measurements of

ACPD
12, 15743–15799, 2012

light penetration and nadir reflectivity of on-shore and off-shore coastal Alaskan snow, J. Geophys. Res., 117, D00R12, doi:10.1029/2011JD016639, 2012.

Frey, M. M., Savarino, J., Morin, S., Erbland, J., and Martins, J. M. F.: Photolysis imprint in the nitrate stable isotope signal in snow and atmosphere of East Antarctica and implications for reactive nitrogen cycling, Atmos. Chem. Phys., 9, 8681–8696, doi:10.5194/acp-9-8681-2009, 2009.

Frey, M. M., Brough, N., France, J. L., King, M. D., Erbland, J., Savarino, J., Anderson, P. S., Jones, A. E., and Wolff, E. W.: Atmospheric nitrogen oxides (NO and NO_2) at Dome C: first observations and implications for reactive nitrogen cycling above the East Antarctic Ice Sheet, in preparation, 2012.

Frieß, U., Deutschmann, T., Gilfedder, B. S., Weller, R., and Platt, U.: Iodine monoxide in the Antarctic snowpack, Atmos. Chem. Phys., 10, 2439–2456, doi:10.5194/acp-10-2439-2010, 2010.

Gallet, J.-C., Domine, F., Arnaud, L., Picard, G., and Savarino, J.: Vertical profiles of the specific surface area and density of the snow at Dome C and on a transect to Dumont D'Urville, Antarctica – albedo calculations and comparison to remote sensing products, The Cryosphere, 5, 631–649, doi:10.5194/tc-5-631-2011, 2011.

Gardiner, B. G. and Martin, T. J.: On measuring and modelling ultraviolet spectral irradiance. in: Current Problems in Atmospheric Radiation, edited by: Smith, W. L. and Stamnes, K., Adarsh Deepak Publishing, 917–920, 1997.

Grannas, A. M., Jones, A. E., Dibb, J., Ammann, M., Anastasio, C., Beine, H. J., Bergin, M., Bottenheim, J., Boxe, C. S., Carver, G., Chen, G., Crawford, J. H., Dominé, F., Frey, M. M., Guzmán, M. I., Heard, D. E., Helmig, D., Hoffmann, M. R., Honrath, R. E., Huey, L. G., Hutterli, M., Jacobi, H. W., Klán, P., Lefer, B., McConnell, J., Plane, J., Sander, R., Savarino, J., Shepson, P. B., Simpson, W. R., Sodeau, J. R., von Glasow, R., Weller, R., Wolff, E. W., and Zhu, T.: An overview of snow photochemistry: evidence, mechanisms and impacts, Atmos. Chem. Phys., 7, 4329–4373, doi:10.5194/acp-7-4329-2007, 2007.

Grenfell, T. C.: A radiative transfer model for sea ice with vertical structure variations, J. Geophys. Res., 96, 16991–17001, 1991.

Grenfell, T. C. and Perovich, D. K.: Radiation absorption coefficients of polycrystalline ice from 400–1400 nm, J. Geophys. Res., 86, 7447–7450, 1981.

ACPD
12, 15743–15799, 2012

Grenfell, T. C., Doherty, S. J., Clarke, A. D., and Warren, S. G.: Light absorption from particulate impurities in snow and ice determined by spectrophotometric analysis of filters, Appl. Optics, 50, 1–13, 2011.

Hansen, J. E. and Travis, L. D.: Light scattering in planetary atmospheres, Space Sci. Rev., 16, 527–610, 1974.

Hoffer, A., Gelencsér, A., Guyon, P., Kiss, G., Schmid, O., Frank, G. P., Artaxo, P., and Andreae, M. O.: Optical properties of humic-like substances (HULIS) in biomass-burning aerosols, Atmos. Chem. Phys., 6, 3563–3570, doi:10.5194/acp-6-3563-2006, 2006.

Honrath, R. E., Peterson, M. C., Guo, S., Dibb, J. E., Shepson, P. B., and Campbell, B.: Evidence of NO_x production within or upon ice particles in the Greenland snowpack, Geophys. Res. Lett., 26, 695–698, 1999.

Honrath, R. E., Lu, Y., Peterson, M. C., Dibb, J. E., Arsenault, M. A., Cullen, N. J., and Steffen, K.: Vertical fluxes of NO_x, HONO, and HNO_3 above the snowpack at Summit, Greenland, Atmos. Environ., 36, 2629–2640, 2002.

Jacob, D. J., Heikes, B. G., Fan, S.-M., Logan, J. A., Mauzerall, D. L., Bradshaw, J. D., Singh, H. B., Gregory, G. L., Talbot, R. W., Blake, D. R., and Sachse, G. W.: Origin of ozone and NO_x in the tropical troposphere: a photochemical analysis of aircraft observations over the South Atlantic basin, J. Geophys. Res., 101, 24235–24250, 1996.

Jacob, D. J.: Heterogeneous chemistry and tropospheric ozone, Atmos. Environ., 34, 2131–2159, 2000.

Johnston, H. and Graham, R.: Gas-phase ultraviolet absorption spectrum of nitric acid vapor, J. Phys. Chem., 77, L13501, 1973.

Jones, A. E., Weller, R., Anderson, P. S., Jacobi, H.-W., Wolff, E. W., Schrems, O., and Miller, H.: Measurements of NO_x emissions from the Antarctic snowpack, Geophys. Res. Lett., 28, 1499–1502, 2001.

Jones, A. E., Wolff, E. W., Ames, D., Bauguitte, S. J.-B., Clemitshaw, K. C., Fleming, Z., Mills, G. P., Saiz-Lopez, A., Salmon, R. A., Sturges, W. T., and Worton, D. R.: The multi-seasonal NO_y budget in coastal Antarctica and its link with surface snow and ice core nitrate: results from the CHABLIS campaign, Atmos. Chem. Phys., 11, 9271–9285, doi:10.5194/acp-11-9271-2011, 2011.

Kirchstetter, T. W., Novakov, T., and Hobbs, P. V.: Evidence that the spectral dependence of light absorption by aerosols is affected by organic carbon, J. Geophys. Res., 109, D21208, doi:10.1029/2004JD004999, 2004.

ACPD
12, 15743–15799, 2012

Liao, J., Huey, L. G., Tanner, D. J., Brough, N., Brooks, S., Dibb, J. E., Stutz, J., Thomas, J. L., Lefer, B., Haman, C., and Gorham, K.: Observations of hydroxyl and peroxy radicals and the impact of BrO at Summit, Greenland in 2007 and 2008, Atmos. Chem. Phys., 11, 8577–8591, doi:10.5194/acp-11-8577-2011, 2011.

Massman, W. J.: A review of the molecular diffusivities of H_2O, CO_2, CO, O_3, SO_2, NH_3, N_2O, NO and NO_2 in air, O_2 and N_2 near STP, Atmos. Environ., 32, 1111–1127, 1998.

Mauldin, R., Kosciuch, E., Eisele, F., Huey, G., Tanner, D., Sjostedt, S., Blake, D., Chen, G., Crawford, J., and Davis, D.: South Pole Antarctica observations and modeling results: new insights on HO_x radical and sulfur chemistry, Atmos. Environ., 44, 572–581, 2010.

Mayewski, P. A. and Legrand, M. R.: Recent increase in nitrate concentration of Antarctic snow, Nature, 346, 258–260, 1990.

Michalowski, B. A., Francisco, J. S., Li, S.-M., Barrie, L. A., Bottenheim, J. W., and Shepson, P. B.: A computer model study of multiphase chemistry in the Arctic boundary layer during polar sunrise, J. Geophys. Res., 105, 15131–15145, 2000.

Mulvaney, R., Wagenbach, D., and Wolff, E. W.: Postdepositional change in snowpack nitrate from observation of year-round near-surface snow in coastal Antarctica, J. Geophys. Res., 103, 11021–11031, 1998.

Oncley, S. P., Buhr, M., Lenschow, D. H., Davis, D., and Semmer, S. R.: Observations of summertime NO fluxes and boundary-layer height at the South Pole during ISCAT 2000 using scalar similarity, Atmos. Environ., 38, 5389–5398, 2004.

Orvig, S.: Climate of the Polar regions. World survey of climatology, vol. 14, Elsevier, 1970.

Perovich, D. K. and Govoni, J. W.: Absorption coefficients of ice from 250 to 400 nm, Geophys. Res. Lett., 18, 1233–1235, 1991.

Pinzer, B. R., Kerbrat, M., Huthwelker, T., Gaggeler, H. W., Schneebeli, M., and Ammann, M.: Diffusion of NO_x and HONO in snow: a laboratory study, J. Geophys. Res., 115, 4147, doi:10.1029/2009JD012459, 2010.

Price, P. and Bergstrom, L.: Optical properties of deep ice at the South Pole: scattering, Appl. Optics, 36, 4181–4194, 1997.

Roden, C. H., Bond, T. C., Conway, S., and Osorto Pinel, A. B.: Emission factors and real-time optical properties of particles emitted from traditional wood burning cookstove, Environ. Sci. Technol., 40, 6750–6757, 2006.

ACPD
12, 15743–15799, 2012

Rothlisberger, R., Hutterli, M. A., Sommer, S., Wolff, E. W., and Mulvaney, R.: Factors controlling nitrate in ice cores: evidence from the Dome C deep ice core, J. Geophys. Res., 105, 20565–20572, 2000.

Sander, S. P., Friedl, R. R., Golden, D. M., Kurylo, M. J., Moortgat, G. K., Keller-Rudek, H., Wine, P. H., Ravishankara, A. R., Kolb, C. E., Molina, M. J., Finlayson-Pitts, B. J., Huie, R. E., and Orkin, V. L.: Chemical Kinetics and Photochemical Data for Use in Atmospheric Studies Evaluation Number 15. JPL Publication, 06–2, 2006.

Savarino, J., Kaiser, J., Morin, S., Sigman, D. M., and Thiemens, M. H.: Nitrogen and oxygen isotopic constraints on the origin of atmospheric nitrate in coastal Antarctica, Atmos. Chem. Phys., 7, 1925–1945, doi:10.5194/acp-7-1925-2007, 2007.

Seinfeld, J. H. and Pandis, S. N.: Atmospheric Chemistry and Physics From Air Pollution to Climate Change. John Wiley & Sons, Inc., 2006.

Sjostedt, S. J., Huey, L. G., Tanner, D. J., Peischl, J., Chen, G., Dibb, J. E., Lefer, B., Hutterli, M. A., Beyersdorf, A. J., Blake, N. J., Blake, D. R., Sueper, D., Ryerson, T., Burkhart, J., and Stohl, A.: Observations of hydroxyl and the sum of peroxy radicals at Summit, Greenland during summer 2003, Atmos. Environ., 41, 5122–5137, 2007.

Slusher, D. L., Huey, L. G., Tanner, D. J., Chen, G., Davis, D. D., Buhr, M., Nowak, J. B., Eisele, F. L., Kosciuch, E., Mauldin, R. L., Lefer, B. L., Shetter, R. E., and Dibb, J. E.: Measurements of pernitric acid at the South Pole during ISCAT 2000, Geophys. Res. Lett., 29, 21, doi:10.1029/2002GL015703, 2002.

Stamnes, K., Tsay, S., Wiscome, and Jayaweera, W.: Numerically stable algorithm for discrete-ordinate-method radiative transfer in multiple scattering and emitting layered media, Appl. Optics, 27, 12, 2502–2509, 1988.

Steffen, K. and Box, J.: Surface climatology of the Greenland ice sheet: Greenland Climate Network 1995–1999, J. Geophys. Res., 106, 33951–33964, 2001.

Stutz, J., Thomas, J. L., Hurlock, S. C., Schneider, M., von Glasow, R., Piot, M., Gorham, K., Burkhart, J. F., Ziemba, L., Dibb, J. E., and Lefer, B. L.: Longpath DOAS observations of surface BrO at Summit, Greenland, Atmos. Chem. Phys., 11, 9899–9910, doi:10.5194/acp-11-9899-2011, 2011.

Thomas, J. L., Stutz, J., Lefer, B., Huey, L. G., Toyota, K., Dibb, J. E., and von Glasow, R.: Modeling chemistry in and above snow at Summit, Greenland – Part 1: Model description and results, Atmos. Chem. Phys., 11, 4899–4914, doi:10.5194/acp-11-4899-2011, 2011.

ACPD
12, 15743–15799, 2012

Thomas, J. L., Dibb, J. E., Huey, L. G., Liao, J., Tanner, D., Lefer, B., von Glasow, R., and Stutz, J.: Modeling chemistry in and above snow at Summit, Greenland – Part 2: Impact of snowpack chemistry on the oxidation capacity of the boundary layer, Atmos. Chem. Phys. Discuss., 12, 5551–5600, doi:10.5194/acpd-12-5551-2012, 2012.

Tie, X., Zhang, R., Brasseur, G., Emmons, L., and Lei, W.: Effects of lightning on reactive nitrogen and nitrogen reservoir species in the troposphere, J. Geophys. Res., 106, 3167–3178, 2001.

Waddington, E. D., Cunningham, J., and Harder, S. L.: The effects of snow ventilation on chemical concentrations, NATO ASI Ser. Ser. I, 43, 404–451, 1996.

Wang, Y., Choi, Y., Zeng, T., Davis, D., Buhr, M., Huey, G. L., and Neff, W.: Assessing the photochemical impact of snow NO_x emissions over Antarctica during ANTCI 2003, Atmos. Environ., 41, 3944–3958, doi:10.1016/j.atmosenv.2007.01.056, 2007.

Warneck, P. and Wurzinger, C.: Product quantum yields for the 305-nm photodecomposition of NO_3^- in aqueous solution, J. Phys. Chem., 92, 6278–6283, doi:10.1021/j00333a022, 1988.

Warren, S. G. and Brandt, R. E.: Optical constants of ice from the ultraviolet to the microwave: a revised compilation, J. Geophys. Res., 113, D14220, doi:10.1029/2007jd009744, 2008.

Warren, S. G. and Clarke, A. D.: Soot in the atmosphere and snow surface of antarctica, J. Geophys. Res., 95, 1811–1816, 1990.

Warren, S. G. and Wiscombe, W. J.: Dirty snow after nuclear war, Nature, 313, 467–470, 1985.

Warren, S. G., Brandt, R. E., and Hinton, P.-O.: Effect of surface roughness on bidirectional reflectance of Antarctic snow, J. Geophys. Res., 103, 25789–25807, 1998.

Warren, S. G., Brandt, R. E., and Grenfell, T. C.: Visible and near-ultraviolet absorption spectrum of ice from transmission of solar radiation into snow, Appl. Optics, 45, 5320–5334, 2006.

Wild, O., Zhu, X., and Prather, M. J.: Fast-J: accurate simulation of in- and below-cloud photolysis in tropospheric chemical models, J. Atmos. Chem., 37, 245–282, 2000.

Wiscombe, W. J.: The delta-*M* method: rapid yet accurate radiative flux calculations for strongly asymmetric phase functions, J. Atmos. Sci., 34, 1408–1422, 1977.

Wiscombe, W. J. and Warren, S. G.: A model for the spectral albedo of snow. I: Pure snow, J. Atmos. Sci., 37, 2712–2733, 1980.

Wolff, E. W., Jones, A. E., Martin, T. J., and Grenfell, T. C.: Modelling photochemical NO_x production and nitrate loss in the upper snowpack of Antarctica, Geophys. Res. Lett., 29, 1944, doi:10.1029/2002GL015823, 2002.

ACPD
12, 15743–15799, 2012

Yang, X., Cox, R. A., Warwick, N. J., Pyle, J. A., Carver, G. D., O'Connor, F. M., and Savage, N. H.: Tropospheric bromine chemistry and its impacts on ozone: a model study, J. Geophys. Res., 110, D2331, doi:10.1029/2005JD006244, 2005.

Zender, C. S., Bian, H., and Newman, D.: The mineral dust entrainment and deposition (DEAD) model: description and 1990s dust climatology, J. Geophys. Res., 108, 4416, doi:10.1029/2002JD002775, 2003.

Zhu, C., Xiang, B., Chu, L. T., and Zhu, L.: 308 nm photolysis of nitric acid in the gas phase, on aluminum surfaces, and on ice films, J. Phys. Chem. A, 114, 2561–2568, doi:10.1021/jp909867a, 2010.

ACPD

12, 15743–15799, 2012

Table 1. Description of snow samples collected near Dome C, Antarctica in January 2004 and Summit, Greenland in June 2007. The average and standard deviation (1σ) of black carbon concentration (C_{BC}), the Angstrom exponent (Å), and the mean fraction of nonBC (f_{nonBC}) absorption in the λ = 650–700 nm and λ = 298–345 nm ranges at Dome C and Summit station are provided along with the number of snow samples (n) collected at each location.

distance from station (km)	C_{BC}(ng g^{-1})	Å	$f_{nonBC\_650–700}$ (%)	$f_{nonBC\_298–345}$ (%)	n
Dome C, Antarctica					
<0.5	2.1 ± 1.3	2.3 ± 0.4	20.0 ± 4.2	85.6 ± 2.9	13
11	0.6 ± 0.2	2.9 ± 0.4	29.0 ± 0.8	88.6 ± 0.8	4
Summit, Greenland					
>20	1.4 ± 0.3	2.7 ± 0.3	29.0 ± 4.9	89.2 ± 2.2	5

ACPD
12, 15743–15799, 2012

Table 2. The correction factor (Corr(μ_0)) used in Eq. (13) and Eq. (15), where μ_0 = cosine of the solar zenith angle (θ).

θ	10°	20°	30°	40°	50°	60°	70°	80°	85°
μ_0	0.985	0.940	0.866	0.766	0.643	0.500	0.342	0.174	0.087
Corr(μ_0)	1.061	1.063	1.063	1.063	1.058	1.047	1.023	0.973	6.993

ACPD
12, 15743–15799, 2012

Table 3. Values for the variables used to calculate the lifetime of NO_x in the snowpack interstitial air against escape to the overlying atmosphere via wind pumping during austral summer at Dome C and South Pole and during summer at Summit. The base-case values are provided along with the range of values used in the sensitivity studies in parentheses.

	Dome C	Summit	South Pole	References
sastrugi height (h, cm)	5.5 (3–8)	5 (3–8)	19.5 (9–25)	Albert and Hawley (2002), Six and Warren, unpublished results (2012), Warren et al. (1998)
sastrugi wavelength (λ, cm)	55 (30–80)[a]	135 (50–225)	170 (70–400)	Albert and Hawley (2002), Six and Warren, unpublished results (2012), Warren et al. (1998)
wind speed (U, $m\,s^{-1}$)[b]	2.8 (1.5–5)	4.3 (2–6)	4.7 (4.2–5.2)	Albert and Hawley (2002), Aristidi et al. (2005), Orvig (1970)

[a] Sastrugi aspect ratio (height/width) of 0.1 using h from unpublished results from Six and Warren to calculate λ at Dome C.
[b] Wind speeds at South Pole from Orvig (1970) are 10-m wind speeds. 10-m wind speeds should be used in Eq. (23) to calculate $\tau_{\text{wind pumping}}$ when available.

ACPD
12, 15743–15799, 2012

Table 4. Chemical concentrations used in the NO_x chemical lifetime ($\tau_{chemical}$) equations. The summertime base-case values of boundary layer [NO_2], [NO], [OH], and [BrO] are provided along with the range of values used in the sensitivity studies in parentheses.

	Dome C	South Pole	Summit	References
[NO_2]	166 (42–290)	175 (0–350)	15 (0–30)	Davis et al. (2004), Frey et al. (2012), Thomas et al. (2011)
[NO]	95 (18–172)	136 (0–550)	25 (0–50)	Davis et al. (2004), Frey et al. (2012), Thomas et al. (2011)
[OH]	0.08 (.033–.13)[a]	0.08 (.033–.13)	0.22 (.14–.28)	Mauldin et al. (2010), Sjostedt et al. (2007)
[BrO]	0.5 (0.25–1)[b]	0.5 (0.25–1)[b]	2 (0–4)	Stutz et al. (2010), Yang et al. (2005)

[a] South Pole [OH] measurements from Mauldin et al. (2010) used at Dome C.
[b] Modeled [BrO] concentrations from Yang et al. (2005) used at Dome C and South Pole.

ACPD
12, 15743–15799, 2012

Table 5. Calculated e-folding depths of actinic flux (z_e) in snow near the station and remote from the station in the designated clean-air sector for January at Dome C and South Pole and June at Summit for λ = 305 nm and λ = 400 nm. The range of e-folding depths represents the range between fully direct (smaller z_e) and fully diffuse (larger z_e) incident radiation conditions. Mean values of C_{BC} from Table 1 were used to calculate z_e at each location.

		Wavelength (λ, nm)		C_{BC}
		305	400	(ng g^{-1})
Dome C	remote	18–22 cm	32–40 cm	0.6
	station	10–12 cm	18–21 cm	2.1
Summit	remote	15–17 cm	23–28 cm	1.4
South Pole	remote	26–31 cm	53–62 cm	0.3
	station	8–10 cm	15–18 cm	3.0

ACPD
12, 15743–15799, 2012

Table 6. Calculated and observed NO_x fluxes (F_{NO_x}) near Dome C, Summit, and South Pole.

	Polar NO_x Fluxes (molecules cm^{-2} s^{-1})			
	Calculations (this work)		Observations	
Location	Remote	Station	Station	Reference
Dome C	4.4×10^8–1.9×10^9	3.2–8.2×10^8	5.3×10^{8a}	France et al. (2011)
Summit	1.3–2.8×10^9		2.5×10^8	Honrath et al. (2002)
South Pole	7.7×10^8–2.2×10^9	3.3–9.8×10^8	2.2–3.8×10^8	Davis et al. (2004) Oncley et al. (2004)

[a] NO_x flux modeled by France et al. (2011) is at the upper end of observed NO_x fluxes ≤5 km from Dome C station (Frey, personal communication, 2011).

ACPD
12, 15743–15799, 2012

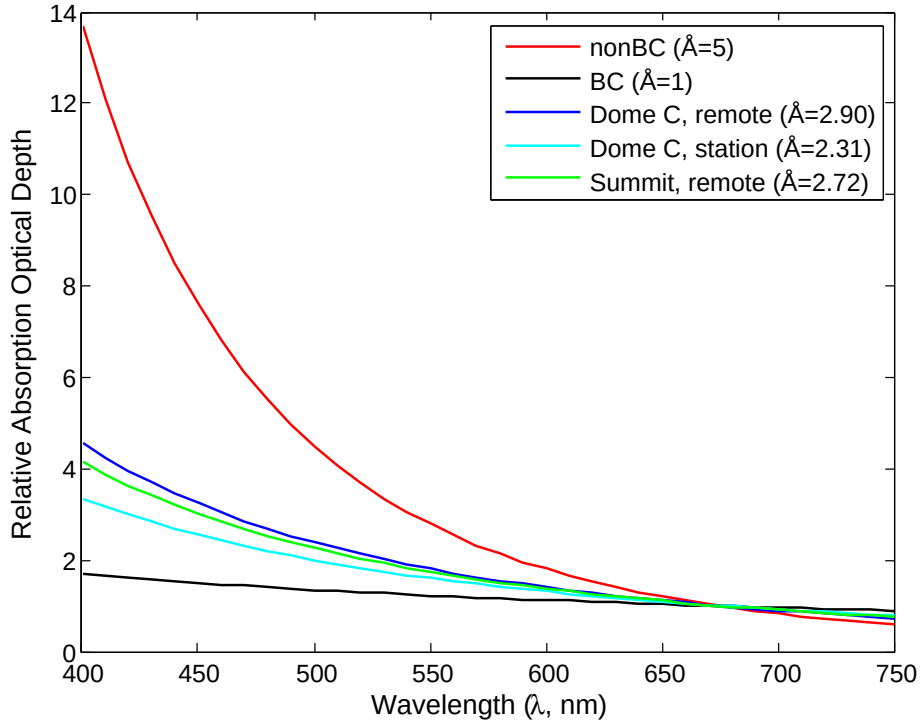

Fig. 1. Idealized absorption profiles (expressed in absorption optical depth, $T(\lambda)$ of BC (black) and nonBC (red) material from Grenfell et al. (2011) and Hoffer et al. (2006). Also shown are absorption profiles of snow samples collected in remote Dome C (blue), remote Summit (green), and near-station Dome C (cyan).

ACPD
12, 15743–15799, 2012

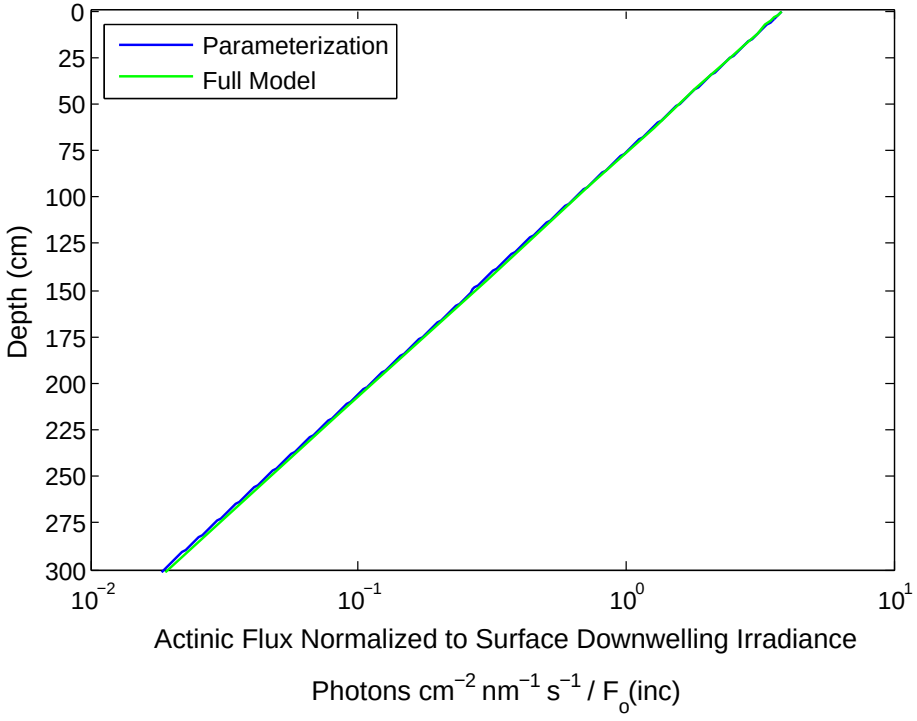

Fig. 2. Actinic flux profile normalized to surface downwelling radiation determined by our parameterization (Eq. 18) and the full model (Grenfell, 1991) for a representative deep (depth >3 m) snowpack. For this comparison, the incident radiation field is entirely diffuse, λ = 305 nm, θ = 60°, r_e = 100 µm, and C_{BC} = 0.3 ng g^{-1}, and C_{nonBC} = 0 ng g^{-1}.

ACPD
12, 15743–15799, 2012

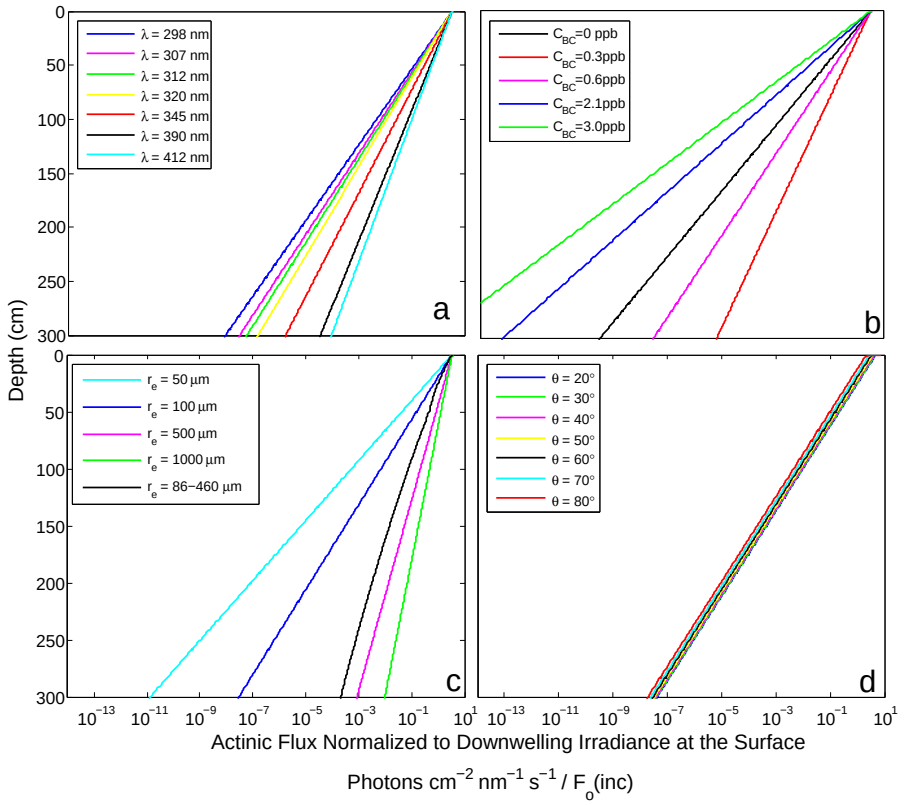

Fig. 3. Dependence of the actinic flux depth profile on wavelength, λ **(a)**, concentration of black carbon in the snowpack, C_{BC} **(b)**, ice grain radius, r_e **(c)**, and solar zenith angle, θ **(d)**. In **(c)**, the black line is the depth profile of actinic flux using vertical r_e profile ranging from 86 µm at the snow surface to 460 µm at a depth of 500 cm. In **(d)**, a zoomed in view of the top 10 cm is provided. In Fig. 3a–d, Å = 2.90 and λ, C_{BC}, r_e, and θ were varied around a reference case of $\theta = 60^\circ$, $r_e = 100\,\mu m$, $\lambda = 305\,nm$, and $C_{BC} = 0.6\,ng\,g^{-1}$.

ACPD
12, 15743–15799, 2012

The influence of snow grain size and impurities

M. C. Zatko et al.

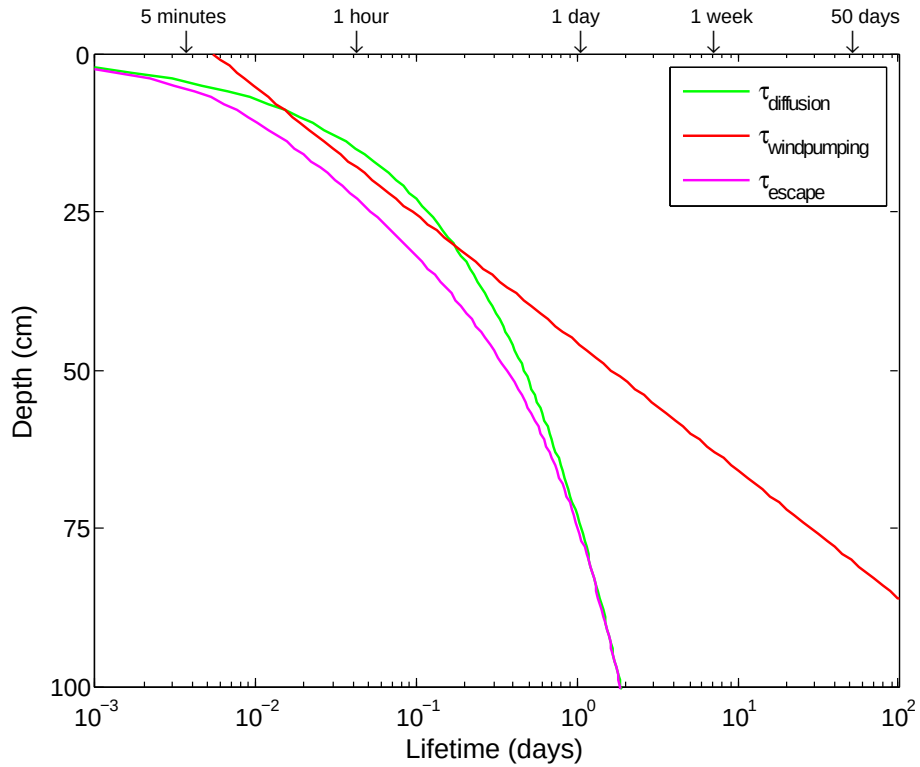

Fig. 4. Calculated lifetime of NO_x in the snowpack against processes responsible for the escape of NO_x from the snowpack interstitial air into the atmosphere at Dome C using base-case values for diffusion (Sect. 2.4) and wind pumping (Table 3). The lifetime of NO_x in the snowpack for diffusion ($\tau_{diffusion}$) is the green curve, the lifetime of NO_x in the snowpack for wind pumping ($\tau_{wind\ pumping}$) is the red curve, and the lifetime of NO_x in the snowpack for the combination of diffusion and wind pumping (τ_{escape}) is the pink curve.

ACPD
12, 15743–15799, 2012

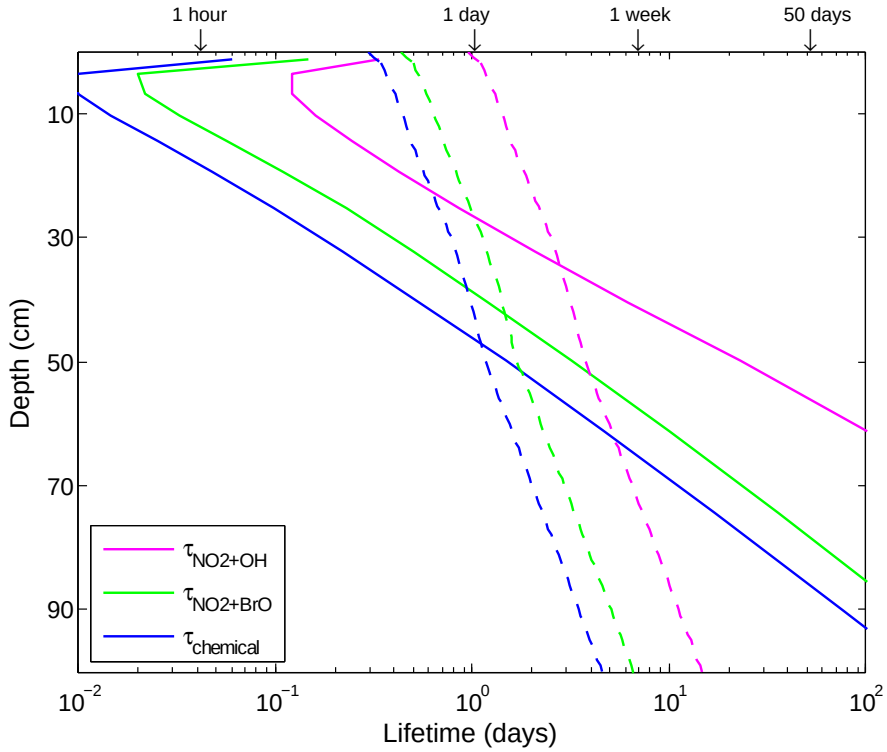

Fig. 5. Depth-dependent lifetime (days) of NO_x in the snowpack against chemical conversion to HNO_3 (τ_{NO_2+OH}, pink curve), $BrONO_2$ (τ_{NO_2+BrO}, cyan curve), and the combination of the two reactions ($\tau_{chemical}$, blue curve) for snow 11 km from Dome C station. The dashed lines use observed concentrations of BrO, OH, NO, and NO_2 at the surface, scaled at depth to the actinic flux at λ = 305 nm. The solid lines use concentration profiles of BrO, OH, NO, and NO_2 from Thomas et al. (2011) scaled to surface observations at Dome C (see Sect. 2.4 for details).

ACPD
12, 15743–15799, 2012

The influence of snow grain size and impurities

M. C. Zatko et al.

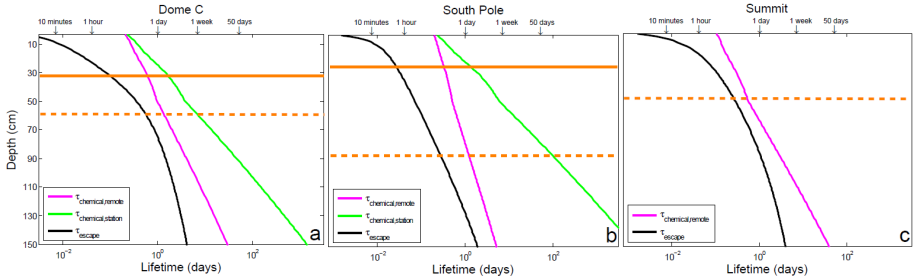

Fig. 6. Vertical profiles of τ_{escape} (black) and τ_{chemical} in snow near the station (green) and far from the station (pink) at Dome C **(a)**, South Pole **(b)**, and Summit **(c)**. The solid orange horizontal lines represent three times the e-folding depth of actinic flux at $\lambda = 305$ nm in snowpack near Dome C and South Pole stations. The dashed orange horizontal lines represent three times the e-folding depth of actinic flux at $\lambda = 305$ nm in snowpack 11 km from Dome C station, 2.5 km from South Pole station, and greater than 20 km from Summit station. The difference between near and far stations snowpacks is the concentrations of impurities, based on observations reported in Table 1.

ACPD
12, 15743–15799, 2012